Performance Analysis of Cascaded RIS-based Communications

Thesis by

Doszhan Zhumabek, B. Eng in Electrical and Computer Engineering

Submitted in fulfilment of the requirements
for the degree of Master of Science
in Electrical and Computer Engineering

Department of Electrical and Computer Engineering
School of Engineering and Digital Sciences
Nazarbayev University

53, Kabanbay Batyr Avenue
Astana, Kazakhstan

Supervisor: Galymzhan Nauryzbayev
Co-supervisor: Gulsim Kulsharova

March 2025

ABSTRACT

This thesis presents a comprehensive performance analysis of cascaded Reconfigurable Intelligent Surface (RIS)-aided communication systems under Nakagami-m fading. It consider a multi-hop (cascaded) RIS architecture, where multiple RIS layers are deployed in series, and incorporate a practical phase shift model that captures the dependency of each reflecting element's amplitude response on its phase adjustment. The aim of this paper is to derive exact analytical expressions for the end-to-end signal-to-noise ratio (SNR) distribution and use them to obtain closed-form formulas for the outage probability (OP) and ergodic capacity (EC) of the cascaded RIS system. To handle the products of multiple fading coefficients and phase responses, the derivations leverage advanced analytical tools such as the Fox H-function and moment-generating function (MGF) methods, yielding tractable expressions for these performance metrics. Monte Carlo simulations validate the accuracy of the derived results across various system configurations. The results demonstrate that imperfect phase alignment due to practical hardware introduces performance degradation compared to the ideal case. Nevertheless, increasing the number of RIS layers and reflecting elements significantly improves SNR, resulting in lower OP and higher EC. These findings highlight the trade-offs between RIS network density (number of layers/elements) and achievable performance under practical phase shift limitations, providing valuable design insights for future beyond 5G (B5G) and sixth generation (6G) cellular networks and cascaded RIS-based wireless networks.

ACKNOWLEDGEMENTS

Firstly, I would like to express my gratitude to my professor and supervisor, Dr. Galymzhan Nauryzbayev, for his support and guidance throughout throughout my master's degree education period. His expertise, constructive feedback, and assistance have been invaluable to me. I deeply appreciate the time and effort he has invested in helping me succeed.

My deepest gratitude is extended to my family for their love, support, and encouragement. To my parents, your belief in me has been a constant source of motivation and strength through all this time. To my dear wife, thank you for your patience, understanding, and for creating perfect conditions for me to focus on my studies. I am grateful for everything you have done to me.

Lastly, I would like to thank my friends for their support and assistance whenever needed. Especially I want to mention Ruslan, who always pushed me to study and motivated me to keep going, when everything seemed difficult.

Contents

LIST OF ABBREVIATIONS

1G	First Generation
2.5G	Second-and-a-half Generation
2G	Second Generation
3G	Third Generation
4G	Fourth Generation
5G	Fifth Generation
6G	Sixth Generation
8-PSK	8-phase Shift Keying
AC	Alternating Current
AR	Augmented Reality
B5G	Beyond 5G
BER	Bit Error Rate
BS	Base Station
CA	Carrier Aggregation
CDF	Cumulative Density Function
COVID-19	Coronavirus Disease 2019
D2D	Device-to-Device Communication
DC	Direct Current
EC	Ergodic Capacity
EDGE	Enhanced Data Rate for Global Evolution
EM	Electromagnetic
FDMA	Frequency Division Multiple Access
FM	Frequency Modulation
FPGA	Field Programmable Gate Array
GMSK	Gaussian Minimum Frequency Shift Keying
GPRS	General Packet Radio Service
GSM	Global System for Mobile Telecommunication
HSPA	High-Speed Packet Access
IoT	Internet of Things
LoS	Line-of-Sight
LTE	Long-Term Evolution
LTE-A	Long-Term Evolution Advanced
M2M	Machine-to-Machine Communication

MATLAB	MATrix LABoratory
MEMS	Micro-Electromechanical System
MGF	Moment Generating Function
MIMO	Multiple-Input and Multiple-Output
mmWave	Millimeter Wave
OFDM	Orthogonal Frequency Division Multiplexing
OP	Outage Probability
PCB	Printed Circuit Board
PDF	Probability Density Function
PIN	Positive-Intrinsic-Negative
RF	Radio Frequency
RIS	Reconfigurable Intelligent Surface
RV	Random Variable
SMS	Short Message Service
SNR	Signal-to-Noise Ratio
TDMA	Time Division Multiple Access
THz	TeraHertz
UAV	Unmanned Aerial Vehicle
VMS	Voice Mail Service
VoLTE	Voice over Long-Term Evolution
VR	Virtual Reality
WCDMA	Wideband Code Division Multiple Access
Wi-Fi	Wireless Fidelity

LIST OF FIGURES

Chapter 1

Introduction

1.1 Evolution of wireless communication

Wireless communication is a crucial part of modern communication, allowing devices to communicate across different applications, including mobile networks, the Internet of Things (IoT), and satellite communications. In this type of communication, there is no need for physical connection (e.g., physical cables); instead, it uses electromagnetic (EM) waves propagating through the air or space to transmit information. Depending on the application and distance, it uses various frequency bands. Low-frequency bands, such as radio waves, are widely used for communication over long distances, while high-frequency bands, such as microwaves and millimeter waves (mmWaves), are used for high-speed data transmission. Examples of these include satellite communications, fifth generation (5G) networks, and Wireless Fidelity (Wi-Fi). The use of these frequency bands for wireless communication ensures reliable, efficient, and scalable connectivity in various domains.

Wireless technology experienced a significant evolution from early radio communication to current 5G and beyond. A new generation of mobile communication has appeared every decade since 1980 [1]. It begins with the introduction of first generation (1G) cellular networks. The idea of cellular networks is that the local area is divided into smaller parts, called cells, and each cell is served by its Base Station (BS) [2]. In these cellular networks, information is sent through analog signals and the peak data transmission rate was 2.4 kilobits per second (kbps), which was appropriate for voice calls [1]. In the 1G technology, the Frequency Modulation (FM) technique was used along with Frequency Division Multiple Access (FDMA) technologies [1]. The FDMA technology allows to multiple users communicate simultaneously, where for each channel 30 kilohertz (kHz) bandwidth was devoted. Due to the usage of analog signals, 1G had several disadvantages, such as no encryption [1], poor voice quality [2], and security [1]. Moreover, since the frequency range of 1G was limited, the FDMA technology usage limited the number of users [3]. Even with these problems, the arrival of 1G networks laid the groundwork for major changes that followed.

The rise of mobile communication also increased the demand for a more efficient and reliable system. To meet the demand, the second generation (2G) mobile communication was developed, which used digital transmission. The first stage of 2G was the introduction of a Global System for Mobile Telecommunication (GSM) technology. In GSM networks, geographic regions are divided into smaller areas called cells, each of which is managed by its BSs. When a user changes its location from one cell to another ongoing communication session is transferred from the current base station to another. This process called handover is the main feature of 2G mobile communication. Additionally, along with digital voice calls, new services, such as Voice Mail Service (VMS) and Short Message Service (SMS) appeared with GSM technology [2]. 2G used Gaussian Minimum Frequency Shift Keying (GMSK) and Time Division Multiple Access (TDMA) technologies, which allows multiple users to share the same frequency channel by dividing it into different time slots for data transmission [1]- [2]. One of the primary disadvantages of GSM was the limited data transmission rate, which ranged from 9.6 kbps to 19.2 kbps [4]. The reason for such a low data rate is the usage of circuit-switching connections, meaning a dedicated channel was reserved for the entire duration of a data session, even when no data was being transmitted. Therefore, a new technology called General Packet Radio Service (GPRS) was developed, which is considered an extension of the 2G technology and called second-and-a-half generation (2.5G) cellular network. In this technology, instead of circuit-switching connections, a packet-switched technology was employed partially, which allowed data to be sent only when needed. This change was reflected in the data transmission rate, which was increased up to 50 kbps [1]. Subsequently, an Enhanced Data Rate for Global Evolution (EDGE) technology was introduced and achieved data rates of 150 kbps to 200 kbps by using an 8-phase Shift Keying (8-PSK) modulation technique [5]. EDGE was introduced in response to the demand for higher data speeds in GSM networks to enable more complex services such as multimedia and internet services. However, despite such advancements, their speed rates still proved to be insufficient for the growing needs of high-speed mobile services, thus leading to the emergence of third generation (3G) cellular network. [5].

The 3G technology introduced significant improvements in terms of data transmission rates and overall network performance. The capability of data transmission enabled a wide array of services, including video calls and streaming, fast internet browsing, and others [3]. 3G mainly uses Wideband Code Division Multiple Access (WCDMA) that enables multiple users to share the same frequency band while minimizing interference and enabling simultaneous transmission of data. Later, High-Speed Packet Access (HSPA) was introduced, which was an improvement of 3G and further enhanced throughput (data rates) by employing a time multiplexing scheme, whereby packets are dynamically scheduled based on network conditions and demand from users. However, despite being several times faster than 2G, 3G was not fast enough to accommodate many growing needs of modern applications, including high-definition video streaming, real-time online gaming, cloud-based services, and others.

To address the limitations of capacity, speed, and network coverage inherent to the 3G networks, Long-Term Evolution (LTE), a fourth generation (4G) cellular networks were created to expand the functionality of the 3G networks [6]. The improvement of such parameters is achieved by using Orthogonal Frequency Division Multiplexing (OFDM), where the communication channel is partitioned into many uniformly spaced frequency bands. User information data is also segmented, and each subcarrier transmits a fraction of this information within a specific frequency band. All these subcarriers remain orthogonal (independent) to one another, even if there is an overlap in uniformly spaced frequency bands [7]. Usage of OFDM allowed to reach the peak speed limits of 50 Megabits per second (Mbps) in the uplink and 100 Mbps in the downlink. Another technology used in 4G is Multiple-Input and Multiple-Output (MIMO), which employs multiple antenna elements at both the transmitter and receiver to enhance the speed and signal quality. The use of MIMO technology in 4G networks enhances overall performance and efficiency in wireless communications [3]. The next generation of LTE is called Long-Term Evolution Advanced (LTE-A). The Carrier Aggregation (CA) technique, which combines multiple frequency bands into a single frequency band, makes it possible to reach the uplink speed of 1 Gigabits per second (Gbps) [6]. One of the significant advancements observed in 4G is the transition from circuit-switching architecture to complete packet-switching, even for voice calls using the new technology - Voice over Long-Term Evolution (VoLTE). Overall, 4G revolutionized mobile communication, providing high-speed data transmission, low latency, and a complete packet switch architecture. Despite its advancements, the demand for ultra-low latency, massive IoT connectivity, and enhanced capacity led to the development of 5G.

The development of 5G networks arises from the limitations of previous generations, which could not meet the increasing demands in terms of speed, latency, and connectivity. The Coronavirus Disease 2019 (COVID-19) pandemic has further highlighted the need for reliable, high-speed communication infrastructure, with an increased number of people switching to remote work, and online education. Due to this, there was a massive increase in data traffic, since for such kinds of activities high-quality video-conferencing, real-time communication, and other tools were vital. Major technologies used in 5G are network slicing [8], Device-to-Device Communication (D2D), Machine-to-Machine Communication (M2M), and Massive MIMO [9]. The data rate of 5G varies between 10 Gbps and 100 Gbps and it ensures latency of less than 1 millisecond (ms) [9]. However, despite these advancements, challenges such as signal blockage in high-frequency bands and power consumption are significant issues for 5G deployment.

The next evolutionary advancement in wireless communication is the sixth generation (6G) of cellular networks, which seeks to improve the capabilities of cellular networks further. 6G networks are expected to provide extremely high speeds, ultra-low latency, widespread connectivity, and improved security and privacy [10]. However, achieving these advancements comes with several critical challenges. One such problem is spectrum scarcity due to the increased number of users resulting in congestion in frequency bands. This encourages exploration of the higher frequency bands, such as mmWave and TeraHertz (THz) frequencies. However, these bands suffer from high propagation loss, signal attenuation, and limited coverage, which makes their adoption difficult [11]. Another problem is the energy efficiency problem since the utilization of technologies like massive MIMO, small cells, and beamforming techniques require significant energy to transmit and process signals. This issue becomes more severe when the number of IoT devices will increase substantially [11]. Moreover, modern wireless communication technologies have issues regarding interference management as more devices operate in the same frequency bands. Regarding these problems, many possible solutions were explored and one of them is a Reconfigurable Intelligent Surface (RIS), which provide a promising solution by optimizing spectrum usage, improving energy efficiency, and reducing interference. Therefore, this thesis examines an important technology towards the development of 6G and provides a comprehensive examination of the performance of RIS-based systems.

1.2 Reconfigurable intelligent surfaces

As the 5G technology continues to be deployed globally and various hardware components for 5G are being developed, researchers are increasingly focusing on advancing technologies for B5G and 6G networks. These next generation networks are expected to offer significant improvements over 5G, such as ultra-low latency, enhanced energy and spectral efficiency, and a broader frequency range, including the mmWave and THz bands [12]. Applications of B5G and 6G networks will include augmented reality (AR), virtual reality (VR), autonomous vehicles, unmanned aerial vehicles (UAVs), smart cities, and many others [12]. A key technology driving the evolution of these networks is RIS, which will play a crucial role in improving network performance and efficiency. RISs are flat surfaces made up of numerous reflecting elements that can independently adjust the amplitude and phase of incoming signals [13]. Typically, RIS is placed between the transmitter and receiver to improve signal strength, reduce interference, and compensate for power losses [13]. Due to these phase shift and amplitude response changes, it is possible to modify the reflected signals in such a way that the intended signal is amplified or interference from other signals at the receiver is minimized [14]. RIS-based communication systems offer many advantages over conventional systems by overcoming obstacles between the transmitter and receiver in both outdoor and indoor environments. Given these attributes, RIS might become one of the key technologies driving expansion B5G and 6G [15].

1.2.1 Hardware structure of RIS

RIS is a planar metasurface composed of many programmable reflecting elements (unit cells) arranged on a substrate with control circuits that tune these elements [13]. Each unit cell can modify the phase amplitude of an incoming EM wave, so that collectively RIS can shape the reflected signals. In hardware terms, RIS is an array of tunable unit cells backed by a supporting structure and managed by an electronic control system.

Practically, these components are realized in a multi-layer Printed Circuit Board (PCB). The top layer contains metallic unit cells, the middle layer is devoted to the bias network and tunable elements, and at the bottom layer control

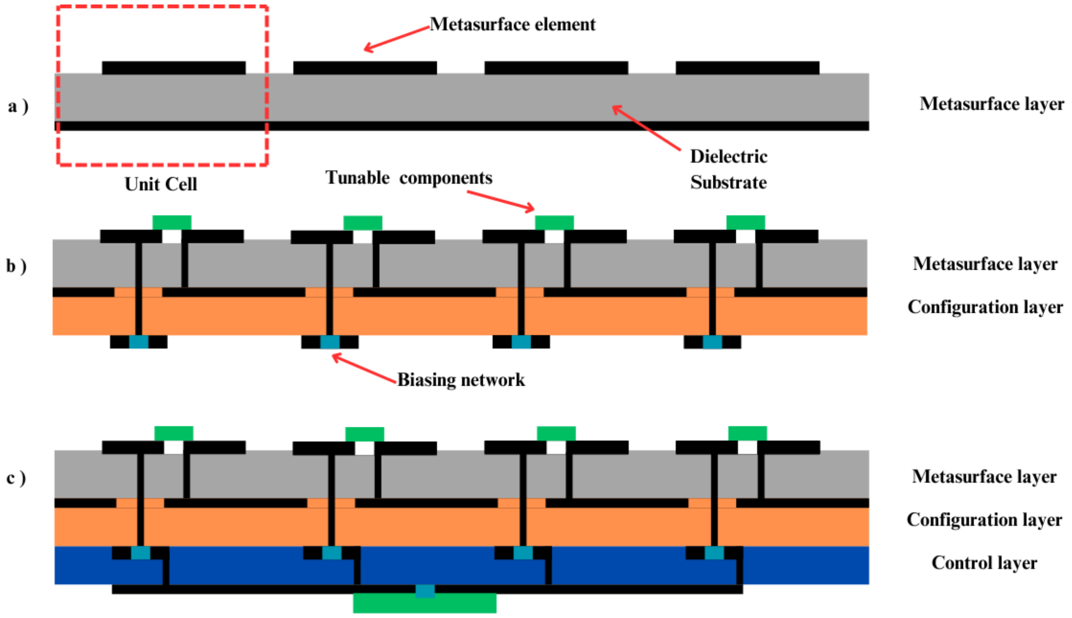

Figure 1.1: Cross-sectional structure of RIS: (a) Schematic of a metasurface layer; (b) Diagram of a reconfigurable metasurface; (c) RIS.

circuitry (microcontroller) is placed [16]. Illustration of the cross-sectional view of a RIS is presented in Figure 1.1.

Unit cells are fundamental elements of RIS. These elements have a small size and perform the main function RIS - reflect the incident EM waves. They are commonly made as flat metal patches (microstrip patch antennas) or other metal shapes on a dielectric material, which serves as a mechanical support [12]. The unit cells are arranged in periodic lattice across the surface with a spacing about half the wavelength or smaller, to uniformly capture the incoming waves. At the bottom of the dielectric substrate, there is a ground plane, which prevents the transmission and maximizes the reflection towards the desired direction. Using the PCB technology to fabricate these patterns makes RIS construction cost effective and scalable [12].

To manipulate the incoming signals, each unit cell is connected to tunable components, which adjusts the effective impedance of resonant frequency. As a tuning element, mostly Positive-Intrinsic-Negative (PIN) diode switches, varactor diodes (variable capacitors), and micro-electromechanical system (MEMS) switches are preferred [12], [16]. These tunable components are integrated into the unit cell design, such that changing their state alters the current flow on the metal patch. Changing the state of the tunable component also results in the change of resonant frequency and impedance, which in turn alters the phase angle of the reflected signal at the operating frequency [12]. For instance, the ON and OFF states of a PIN diode can produce two distinct resonant modes of the cell, corresponding to two discrete phase values (e.g. 0° and 180°) [16]. Using multiple switches or variable reactances can realize multi-bit phase control (more than two states) or even continuous phase tuning in the case of varactors [12].

For the control purposes of the tunable elements, there is a need for a bias network. The bias network is responsible for the delivery of control signals to the tuning elements. This bias network can be implemented as patterned conductive traces which are connected to the unit cell's tuning components. Often there is a specific PCB layer devoted to the bias network called configuration layer. Bias networks sometimes could radiate unwanted signals affecting the radio frequency (RF) performance, therefore design of biasing networks must ensure that it has minimal impact to avoid interference, which is realized by the usage of high-impedance lines or RF chokes. Moreover, each unit cell may have an RF-decoupling network to isolate the control line at RF frequencies while allowing direct current (DC) and alternating current (AC) bias to tune the element. The bias network is a crucial hardware component that links the metasurface layer with the control layer of RIS [16].

The main processing unit of RIS is a control circuit, which is typically implemented by a microcontroller or FPGA-based control board attached to the metasurface [12]. These units control the bias networks using specific algorithms. The control board often communicates with the network (e.g., via a wired connection or wirelessly) to receive configuration commands, effectively making the RIS a controllable network node. Importantly, the control electronics layer is isolated from the RF layer by the substrate and ground, but connected through the bias networks [16].

In summary, the hardware of RISs combines conventional antenna engineering with innovative reconfigurable technologies. The primary components of the RIS hardware (the tunable cells, the substrate structure, and the control/bias circuitry) work together to create specific phase shifts throughout the surface, actively altering how incident waves propagate.

1.2.2 Operating modes of RIS

RIS is a new network entity that consists of a surface capable of reflecting and transmitting signals. It is controlled by an RIS controller, which allows it to operate passively or actively transforming the wireless environment. This transformation enables RIS to turn from a passive element into an intelligent device that can adjust and optimize the communication channel [16]. In the literature, there are six operating modes of RIS: reflection, refraction, absorption, backscattering, transmitting, and receiving mode. However, the majority of research focuses on reflection and refraction modes, while other working modes receive comparatively less attention.

In reflective mode, RIS operates as a surface that reflects EM waves, which is one of the most common applications of RIS. By adjusting the amplitude response and phase shift, RIS directs incoming signals to specific locations, thereby improving the coverage. It is beneficial in cases where direct communication between the BS and end-user is blocked by physical obstacles. Using reflection mode it is possible to create virtual Line-of-Sight (LoS) communication overcoming the barrier between transmitter and receiver, which is particularly useful in urban areas. Furthermore, in reflective mode, it is possible to reduce interference and increase capacity, further optimizing the network performance [12].

Refraction mode enables RIS to control the direction of EM waves when they pass through the surface. Similarly, by manipulating the phase and amplitude of incoming signals, it can refract and redirect the incoming signal in various directions. One of the utilization cases of this mode is outdoor-to-indoor scenario,

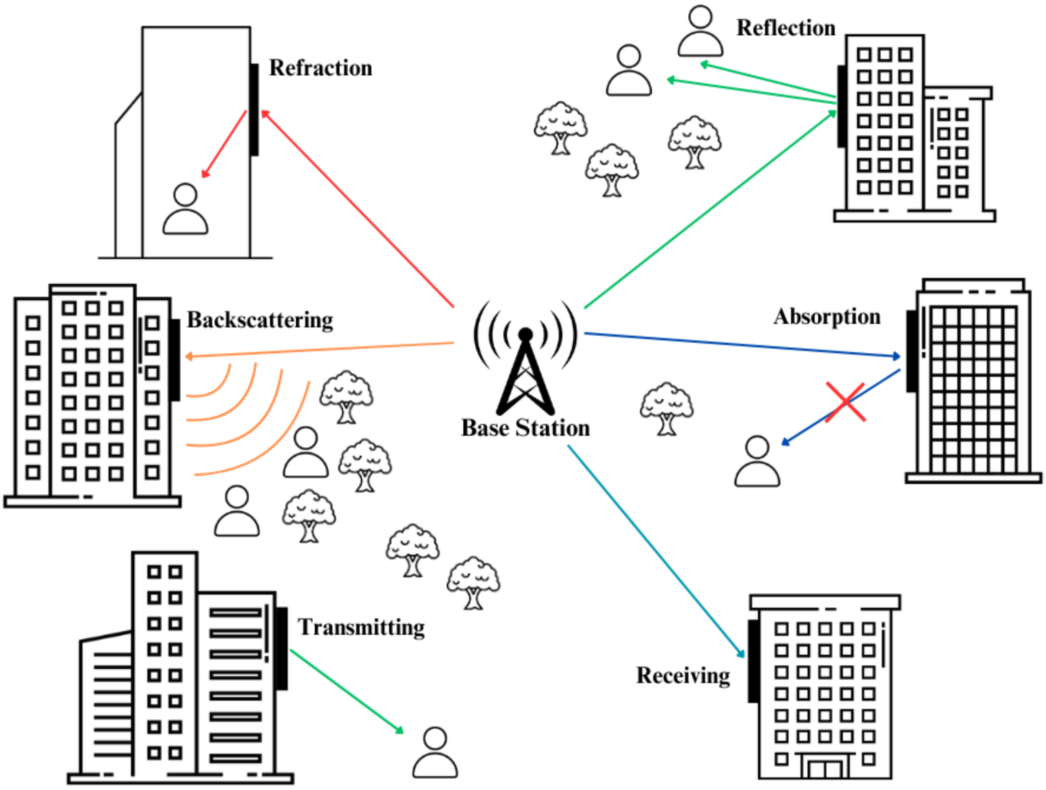

Figure 1.2: Operating modes of RIS.

where RIS can be strategically placed on the external side of a building and redirect the incoming signals to the end-users inside the building. This mode is effective in enhancing the signal quality in indoor environments, when LoS paths are blocked by building layouts [12].

The following working modes of RIS are less popular, but still could be efficient in specific cases. Absorption mode is used when RIS is needed to absorb the signals of specific frequencies, which will be helpful to reduce interference. In crowded communication environments, it can absorb unwanted signals, thus helping to create cleaner and more efficient channels. This mode can be used to improve privacy and security by isolating specific areas from EM waves [16]. In backscattering mode, RIS reflects signals over larger areas rather than targeting specific locations, assisting in reducing blind spots in regions with limited signal coverage [16]. Transmitting mode enables RIS to work similarly to a conventional antenna. RIS in this mode can actively transmit EM waves. This mode integrates RIS with wireless transmitters and utilizes its dynamic metasurface antenna properties, allowing RIS to send signals out to a desired location [16]. In receiving mode, RIS can be used to receive signals from the network performing the opposite role to transmitting. Instead of just reflecting or transmitting, RIS can capture incoming signals and process them, acting as a receiver [16]. Illustration of the working modes of RIS are presented in Figure 1.2.

In conclusion, the diverse operating modes of RIS offer a flexible and efficient means of optimizing wireless network performance, with each mode serving specific needs and contributing to the overall improvement of network performance.

1.2.3 Types of RIS

Based on the power consumption of RIS it could be categorized into passive and active RISs. Structures of both types of RIS are presented in Figures 1.3 and 1.4.

A passive RIS uses no active amplification. Its unit cells only introduce phase shifts through passive components. In hardware terms, each element is a reflective patch combined with a tunable impedance circuit but no transistor-based amplifiers. As a result, passive RIS elements consume virtually zero DC power and generate negligible additional noise [16]. Power is only needed for the control biasing and the control board itself. The benefit of this purely passive approach is simplicity and energy efficiency, which enables RIS to be deployed without heavy power consumption and with minimal thermal considerations. However, passive RIS can only redirect the energy that arrives and they cannot boost or process the signal. In scenarios where the path loss is severe, a passive RIS's reflected signal may be very weak, since it suffers a multiplicative fading effect from the two-hop path (BS-RIS and RIS-user) [17]. Despite this limitation, passive RIS can significantly improve the coverage in indoor and small-cell scenarios, validating their effectiveness when properly designed.

Active RIS incorporates power-consuming active components within its unit cells to amplify the incoming signal. From a hardware perspective, this means each cell contains an amplifier in addition to the passive resonator. A reflection

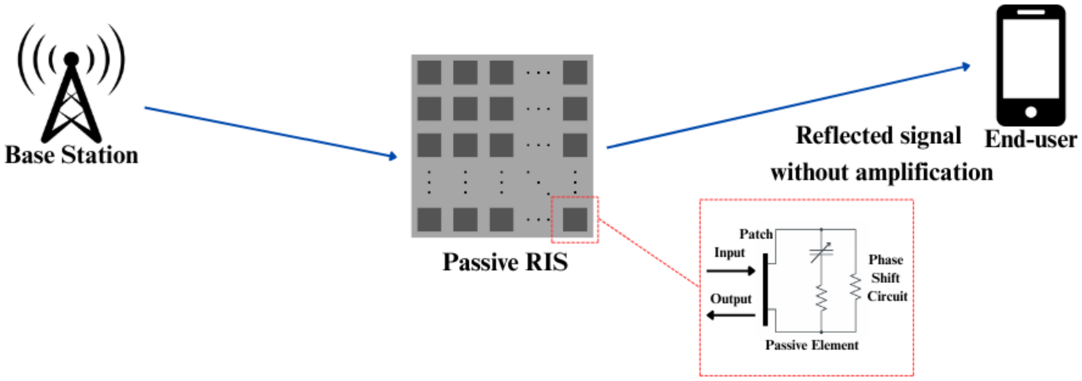

Figure 1.3: Passive RIS structure.

amplifier can be realized with a transistor biased such that it reflects an incident signal with gain. By integrating these into the metasurface, active RIS can add energy into the reflected wave, compensating for path loss [18]. This capability comes at the cost of more complex hardware, such as distribution of DC power to all elements, thermal management of the active devices, and additional control to avoid instability. Active RIS elements also introduce electronic noise, which means the reflected signal will carry some added noise that can reduce the end-to-end SNR [18]. Moreover, active circuits increase the risk of nonlinear effects and interference if not properly isolated. In summary, active RIS hardware aims to overcome the inherent loss of passive reflection by boosting signal strength. Early prototypes of active RIS have shown improved coverage, but they require careful design to balance signal gain against power consumption and noise, and their hardware is significantly more expensive and power-hungry than passive RIS [18].

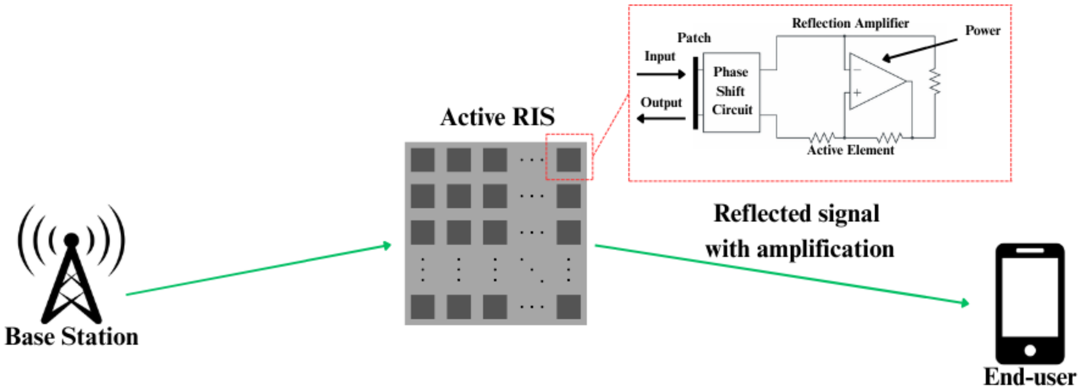

Figure 1.4: Active RIS structure.

In conclusion, RIS offer a new approach to enhancing wireless communication by enabling control over signal reflection and transmission. With their ability to improve coverage, reduce interference, and increase energy efficiency, RIS is poised to play a crucial role in the development of B5G and 6G networks, providing a versatile solution for future communication systems.

1.3 Cascaded channels

Cascaded channels are a series of communication channels connected in a sequence where the output of one channel serves as the input to the next. In a cascaded channel model, each channel introduces its own distortions, noise, and attenuation, which can accumulate as the signal travels through multiple stages. In practical implementations, cascaded channels are often modeled to account for fading, interference, and path loss, which are typical challenges in wireless communication environments. The use of cascaded channels is also important in scenarios like relaying, where intermediate nodes or devices help in forwarding the signal, thus forming a series of links. The study of cascaded channels is essential in the design of advanced communication systems using RISs, which aims to shape the propagation environment. By addressing the complexities of signal propagation across multiple stages and ensuring that the effects of noise, interference, and distortion are minimized, researchers and engineers can significantly improve the performance of modern communication systems, making them more reliable and efficient in various real-world applications.

1.4 Practical phase shift model

In practical implementations, RIS is usually constructed using the PCB, where the metamaterial reflecting elements are periodically placed on a dielectric substrate. These reflecting elements are controlled by semiconductor devices (PIN diodes, varactor diodes, etc.) by varying biasing voltages, which change the impedance of reflecting elements and their resonant frequency. The physical sizes

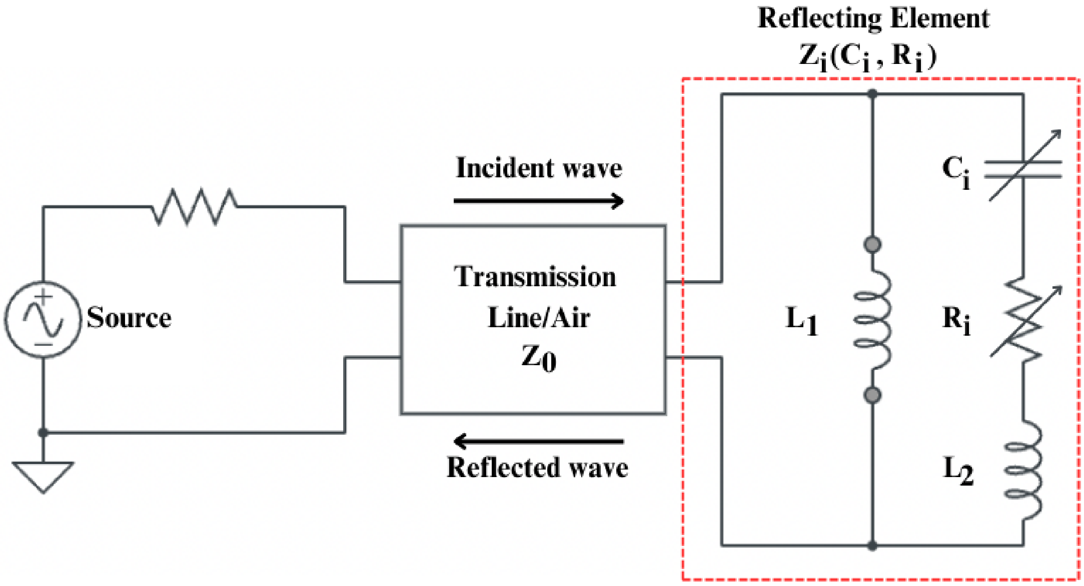

Figure 1.5: An equivalent circuit model of reflecting element of RIS.

of such reflecting elements are typically smaller than the wavelength of the incoming signals. Therefore, its response can be accurately described by a lumped circuit model presented in Figure 1.5 [19].

In this model, metal components of reflecting elements can be designed by inductors, since the high frequency current through these components creates magnetic fields. For the *i*-th reflecting element of a particular intelligent surface, its impedance can be written as

$$Z_i(C_i, R_i) = \frac{j\omega L_1 \left(\omega L_2 + \frac{1}{j\omega C_i} + R_i\right)}{j\omega L_1 + \left(\omega L_2 + \frac{1}{j\omega C_i} + R_i\right)}, \tag{1.1}$$

where, L_1 and L_1 are inductances of the bottom and top layers, respectively. R_i is the effective resistance, which estimates the power dissipation caused by losses in semiconductor devices, metallic parts, and dielectric substrates. C_i is the effective capacitance, which defines the charge accumulation related to the geometry of the element and the semiconductor device. ω is the angular frequency of the incident signal. Then the reflection coefficient can be defined as a parameter that represents the proportion of the reflected EM wave caused by the impedance mismatch between the free space impedance Z_0 and the element impedance $Z_i(C_i, R_i)$:

$$v_i = \frac{Z_i(C_i, R_i) - Z_0}{Z_i(C_i, R_i) + Z_0}. \tag{1.2}$$

Here, it can be observed that the reflection coefficient is a function of the effective capacitance and resistance. By varying these parameters, the reflected EM waves can be controlled. In [19], the authors have shown this dependence experimentally and characterized the relationship between the reflection amplitude and phase shift as

$$\rho_i(\alpha_i) = (1 - \kappa_{\min}) \left(\frac{\sin(\alpha_i - \vartheta) + 1}{2} \right)^{\xi} + \kappa_{\min}. \tag{1.3}$$

Reflection coefficient is defined as $v_i = \rho_i(\alpha_i) e^{j\alpha_i}$, where $\rho_i(\alpha_i) \in [0, 1]$ is the reflection amplitude and $\alpha_i \in [-\pi, \pi)$ is the phase shift of an i-th element of RIS. $\kappa_{\min} \geq 0$, $\vartheta \geq 0$, and $\xi \geq 0$ are specific constants related to circuit implementation and they are responsible for the shape of the dependence curve. Practically, these parameters are fixed once RIS is fabricated, and simple curve fitting tool can help to estimate those parameters [19]. It is also worth to note that when $\kappa_{\min} = 1$ or $\xi = 0$ this circuit acts as an ideal reflector with reflection coefficient equal to unity $\rho_i(\alpha_i) = 1$.

1.5 Literature review

Several researches have recently examined the performance of RIS-based communication systems. Performance metrics, such as coverage, Outage Probability (OP) [20, 21, 22, 23, 24], Bit Error Rate (BER) [22, 24], Ergodic Capacity (EC) [20, 21, 23] were studied over various fading channels (Nakagami-m [24], Rician [20], Rayleigh [21]) with a single RIS system model.

The amount of literature on cascaded RIS systems, which utilize multiple RISs in series to establish a multi-hop pathway, is limited yet expanding. The authors in [2] provided one of the few comprehensive studies in this area. They suggested an effective method to estimate the channel distribution of cascaded RIS-aided wireless networks that takes phase errors over Nakagami-m fading channels into account. This study comes out with closed-form equations for the Probability Density Function (PDF) and the probability of an outage in cascaded RIS systems. The Monte Carlo simulations were used to prove that these expressions were correct. However, in this approximation, the ideal constant reflection coefficient was used, while practically it is difficult to realize such assumption. Therefore, the authors in [19] proposed practical phase shift model in which the amplitude response is dependent on the phase shift. Then, this model was used by [21] and exact expressions of performance metrics, such as OP and EC, were derived. A detailed summary of the literature made on the single RIS system model is presented in [24]. Another study that investigated cascaded RIS is [25], where the authors used OP, EC, and average BER performance metrics and calculated their exact expressions for three cascaded RISs. These results were validated using Monte Carlo simulations, and authors concluded from the results, that in some cases, multiple RIS system models could outperform single-RIS system models [21], if the correct number of RIS was be chosen and coverage of the network could be expanded. In summary, although research on cascaded RIS system models is small relative to single-RIS system models, these investigations reveal the potential of multi-RIS configurations to improve network coverage, offering important insights for forthcoming wireless communication technologies.

1.6 Aims and objectives

Initial aim of this research is to conduct a comprehensive exploration of RIS technology, including the examination of fundamental principles of RIS, its potential application in wireless communication systems, and assessing the impact on enhancing network performance. The research will focus on understanding how RIS can be used to improve the signal propagation, reduction of interference and optimization of network's coverage and capacity. This will provide foundational knowledge, which will guide the following analysis. Second aim of this research is to assess the performance of RIS-aided communication systems using performance metrics, such as OP and EC. Lastly, it was aimed to assess the technical challenges with deploying RIS technology and propose practical solutions to overcome these obstacles. By investigating these aspects, the study seeks to highlight how RIS can play a critical role in enhancing the performance and sustainability of future network infrastructures.

To fulfill the previously stated aims, the following specific objectives will be undertaken. First, an in-depth literature review needs to be carried out, which includes scientific and conference papers, to get relevant insights and research findings about this field. Secondly, using the acquired knowledge cascaded RIS-aided system model will be thoroughly explored. Particularly, it will be attempted to get the exact expression of the signal-to-noise ratio (SNR) of the corresponding model with the practical phase shift assumption, which will be followed by deriving exact expressions for OP and EC. To check the validity of the derived expressions, Monte Carlo simulations will be carried out using MATrix LABoratory (MATLAB) software.

Chapter 2

Methodology

2.1 System model

This research will focus on theoretical investigation of the cascaded RIS system model presented in Figure 2.1. This system model is composed of a transmitter, n cascaded RIS, and an end-user. Additionally, in this system model, it will be assumed that there is no direct link between the transmitter and end-user (receiver). Moreover, signal from the transmitter reaches only the first RIS and direct links between transmitter and other RISs are blocked. Similarly, end-user only receives a signal from the last RIS, while the connections between the receiver and other RISs are also blocked. In order to get performance metrics, such as OP and EC, it is needed to have the distribution of an instantaneous end-to-end SNR. Therefore, let's describe this system model step-by-step, starting from the random channel between the transmitter and RIS 1, which is expressed as

$$h = |h_i| e^{j\phi_i}, \tag{2.1}$$

where $h \in \mathbb{C}^{N_1 \times 1} = \{|h_i| e^{j\phi_i}, \forall i \in N_1\}$, in other words, this random channel is described by the set of N_1 complex Random Variables (RVs), where N_1 is the number of reflecting elements in the RIS 1. Similarly, the random channel between two neighboring RISs is described by

$$G_j = |g_{il}| e^{j\theta_{il}}, \tag{2.2}$$

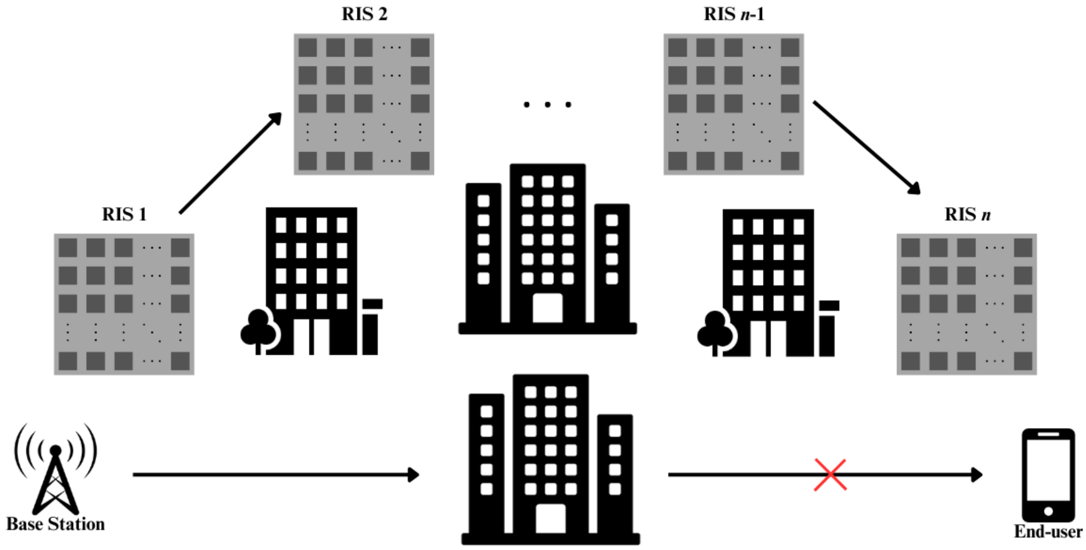

Figure 2.1: Cascaded RIS-aided system model.

where $G_1 \in \mathbb{C}^{N_i \times N_j} = \{|g_{il}^{G_1}|e^{j\theta_{il}^{G_1}}, \forall i \in N_i, \forall j \in N_j\}$. This random channel is described by the set of $N_i \times N_j$ complex RVs, where N_i and N_j are the numbers of elements of RISs i and j, respectively. Finally, the random channel between the last RIS and end-user is shown as

$$q = |q_k|e^{j\psi_k}. \tag{2.3}$$

In the same way, here $q \in \mathbb{C}^{1\times N_k} = \{|q_k|e^{j\psi_k}, \forall k \in N_k\}$ or this random channel is described by the set of N_k complex RVs, where N_k is the number of reflecting elements of last RIS k. It is worth to note that in this system model number of reflecting elements in each RIS is assumed to be same the ($N = N_1 = N_2 = \cdots = N_n$). Each random channel's amplitude are sampled from the i.n.i.d (independent and not necessarily identically distributed) Nakagami-m distribution, which can be modeled as [26]:

$$f_{X_i}(x) = \frac{2m_i^{m_i}}{\Gamma(m_i)\Omega_i^{mi}} x^{2m_i-1} e^{-\frac{m_i}{\Omega_i}x^2}, \quad x \geq 0, \tag{2.4}$$

where, $m_i \geq \frac{1}{2}$ and $\Omega_i > 0$ are the shape and scale parameters of the Nakagami-m distribution, and $\Gamma(\cdot)$ is the Gamma function. Using this system model, an effective signal received by the end-user could be written as [14]:

$$\begin{aligned} y_R = \sum_{i=1}^{N}\sum_{l=1}^{N}\cdots\sum_{j=1}^{N}\sum_{k=1}^{N}\sqrt{\frac{P}{d^{\tau}_{TR_1}d^{\tau}_{R_1R_2}\cdots d^{\tau}_{R_{n-1}R_n}d^{\tau}_{R_nR}}}\times \\ \times |h_i||\eta_i^{R_1}||g_{il}^{G_1}|\cdots|g_{jk}^{G_{n-1}}||\eta_k^{R_n}||q_k|\times \\ \times e^{j\left(\phi_i-\alpha_i^{R_1}+\theta_{il}^{G_1}+\cdots+\theta_{jk}^{G_{n-1}}-\alpha_k^{R_n}+\psi_k\right)}\chi+n_G. \end{aligned} \tag{2.5}$$

This equation describes the cascaded RIS system model, and the definitions will be represented further [14]. Corresponding distances between all entities in this system model will be noted as $d^{\tau}_{TR_1}$, $d^{\tau}_{R_1R_2}$, …, $d^{\tau}_{R_{n-1}R_n}$, $d^{\tau}_{R_nR}$. where R_i in the subscripts meaning the i-th RIS. P is the power of the signal at the transmitter, χ is the signal sent at the transmitter, n_G is the added Gaussian noise (zero mean and σ_R^2 variance), and τ is the path-loss coefficient. In this system model it is also assumed that all connections between entities have the same path-loss coefficient. Additinally, each element of the RIS has an impact on the received signal called the reflection coefficient. This impact is represented by

$$\eta^{R_t} = |\eta_i^{R_t}|e^{-j\alpha_i^{R_t}}, \tag{2.6}$$

where $\eta^{R_t} \in \mathbb{C}^{1\times N_t} = \{|\eta_i^{R_t}|e^{-j\alpha_i^{R_t}}, \forall i \in N_t\}$. This reflection coefficients are represented by the set of complex RVs of size N_t, where N_t is the number of elements of RIS t. The magnitude of the reflection coefficient $|\eta_i^{R_t}|$ is the amplitude, while the exponential part $(e^{-j\alpha_i^{R_t}})$ is the phase shift of i-th element of t-th RIS. Ideally, the magnitude of the reflection coefficient of the RIS is unity; however, practically, there is some relationship between the amplitude and phase responses [19]. Considering this relationship, the reflection coefficient $v_i^{R_t}$ of the i-th element of t-th RIS can be rewritten as

$$v_i^{R_t} = \rho_i^{R_t}(\alpha_i^{R_t})e^{-j\alpha_i^{R_t}}, \tag{2.7}$$

where amplitude response $\rho_i^{R_t}(\alpha_i^{R_t})$ is a function of the phase shift $\alpha_i^{R_t}$, and this function is represented as follows [19]

$$\rho_i^{R_t}(\alpha_i^{R_t}) = (1-\kappa_{\min})\left(\frac{\sin(\alpha_i^{R_t}-\vartheta)+1}{2}\right)^{\xi} + \kappa_{\min}. \tag{2.8}$$

Here, $\kappa_{\min} \geq 0$, $\vartheta \geq 0$, and $\xi \geq 0$ are specific constants, which are related to practical phase shift circuit [19]. $\kappa_{\min}$ is the minimum amplitude, ϑ is the horizontal distance between $-\pi/2$ and $\kappa_{\min}$. Using ξ, it is possible to control the steepness of the curve of practical phase shift. In this system $\alpha_i^{R_t}$ varies between $[-\pi, \pi)$, consequently, $\rho_i^{R_t}(\alpha_i^{R_t})$ will take values between $[0, 1]$ [19]. Usually, it is assumed that these constant parameters are same for all reflective elements. Then, continuing, SNR of the end-to-end system will be expressed as

$$\gamma_R = \frac{\left|\overline{P}\sum_{i=1}^{N}\sum_{l=1}^{N}\cdots\sum_{j=1}^{N}\sum_{k=1}^{N} X_{il\cdots jk}e^{j\delta_{il\cdots jk}}\right|^2}{\sigma^2}. \tag{2.9}$$

Here, $\overline{P}$ stands for the normalized transmit power and defined as

$$\overline{P} = \sqrt{\frac{P}{d_{TR_1}^T d_{R_1R_2}^T \cdots d_{R_{n-1}R_n}^T d_{R_nR}^T}}. \tag{2.10}$$

$X_{il\cdots jk}$ is the product of amplitudes of random channels and reflection coefficient of RISs

$$X_{il\cdots jk} = |h_i||\eta_i^{R_1}||g_{il}^{G_1}|\cdots|g_{jk}^{G_{n-1}}||\eta_k^{R_n}||q_k|, \tag{2.11}$$

and $\delta_{il\cdots jk}$ is the sum of the phases of random channels and reflection coefficients

$$\delta_{il\cdots jk} = \phi_i - \alpha_i^{R_1} + \theta_{il}^{G_1} + \cdots + \theta_{jk}^{G_{n-1}} - \alpha_k^{R_n} + \psi_k. \tag{2.12}$$

In cascaded RIS-aided system, it is impossible to have zero phase error due to several reasons. First of all, at a certain time RIS can modify only one phase of particular path, while the number of path created in such system model depends on number of elements and number of RISs by N^n. Considering this, it could be

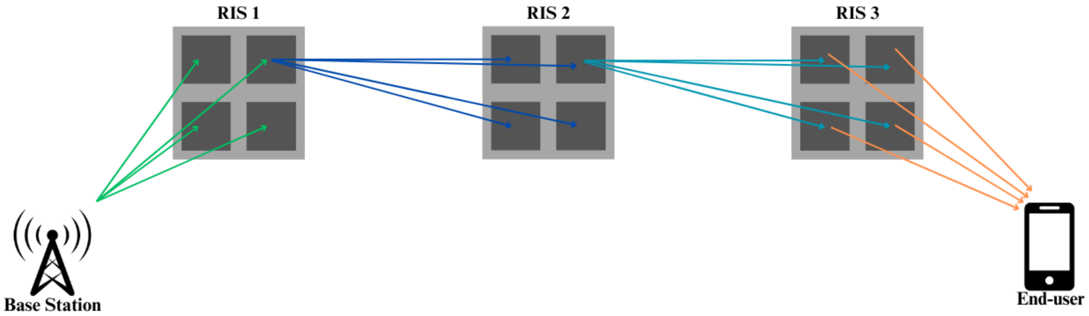

Figure 2.2: Three cascaded RISs each with four reflecting elements.

stated that RIS can only adjust $N \times n$ number of phases, while $N^n - (N \times n)$ phases will have some phase error. As an example, consider simple cascaded RIS-based system model with three RISs each with four reflecting elements presented in Figure 2.2. It can be seen that in this system model, 64 connections are established between the BS and the end-user, with only 12 reflecting elements available to adjust the phases. These 12 reflecting elements can minimize the phase error for one particular path each, leaving 48 paths with some phase error. However, by optimizing the phase contributions of the RIS reflecting elements, it is possible to minimize the overall phase error of the system model. Another reason is that, practically, RIS is limited by the discrete set of phase adjustments depending on number of bits of reflecting elements. This dependence is expressed by

$$Q = 2^b, \tag{2.13}$$

where Q is the number of available phases and b is the number of bits of reflecting elements. As an example consider 2-bit RIS element, where number of available phases is four. Then suppose signal is coming through the random channel to that reflecting element, since RIS have only limited discrete set of available phases, likely there will be phase error because the phase of the random channel could be in the range of 0 and 2π. This can be illustrated by employing unit circle as in Figures 2.3 and 2.4, where blue points are discrete phases of RIS. To better understand and visualize this, consider incoming signal that passes through a random channel with a phase of 2.98 radians (rad) (a red point in Figures 2.3

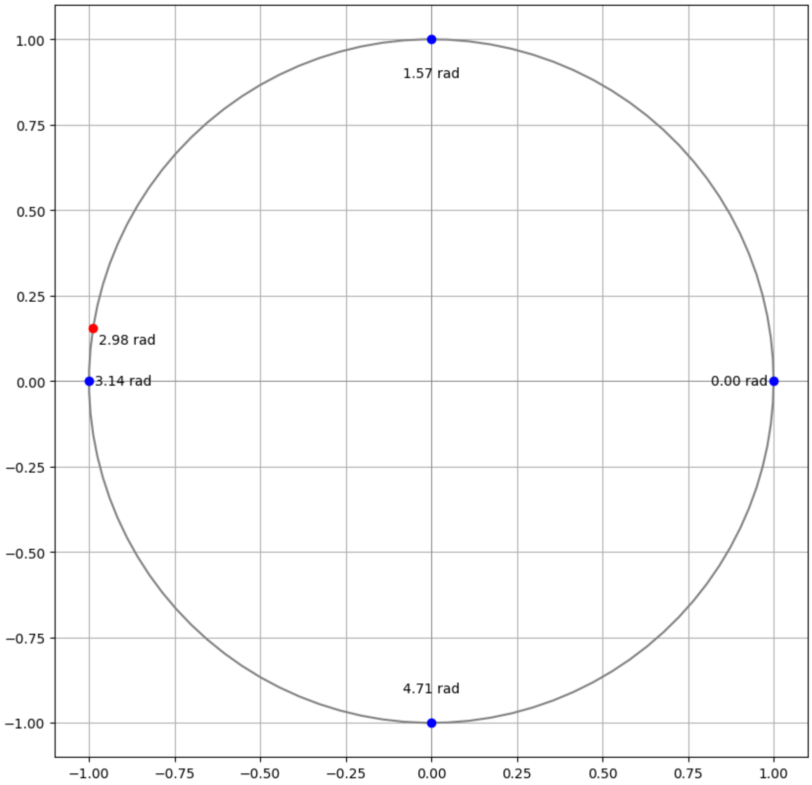

Figure 2.3: Unit circle illustration of RIS phase quantization with 2-bit reflecting elements.

and 2.4) and received by RIS. Due to the discrete phase levels available in the RIS reflecting elements, the phase of the signal must be quantized. As a result, the closest available phase level is selected (π rad in this case in Figures 2.3 and 2.4), introducing a phase error between the incoming signal and the adjusted phase (0.16 rad). Considering these reasons, the phase error at the end-user definitely will be non-zero and will be described by the following uniform distribution

$$f_{\delta_{il\ldots k}}(\delta) = \frac{Q}{2\pi}, \quad -\frac{\pi}{Q} \leq \delta \leq \frac{\pi}{Q}. \tag{2.14}$$

Then SNR (γ_R) can be used to find OP (P_{out}) as [27]

$$P_{\text{out}} = P(\gamma_R < \gamma_{\text{th}}) = \int_0^{\gamma_{\text{th}}} f_{\gamma_R}(\gamma)\,\mathrm{d}\gamma, \tag{2.15}$$

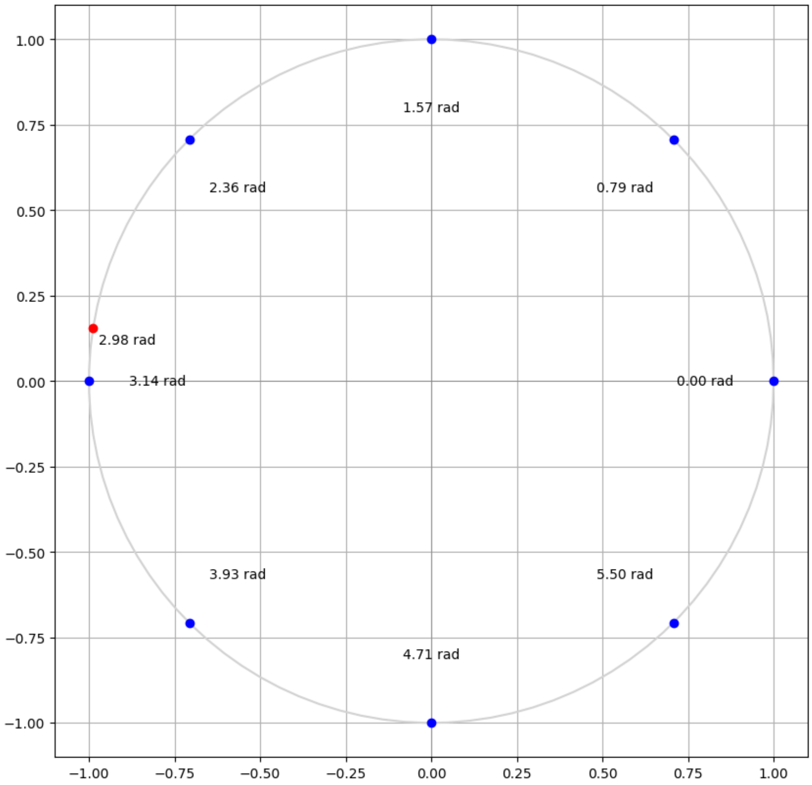

Figure 2.4: Unit circle illustration of RIS phase quantization with 3-bit reflecting elements.

and EC (C_{erg}) could be found as [28]

$$C_{\text{erg}} = \mathbb{E}[\log_2(1+\gamma_R)] = \int_0^\infty \log_2(1+\gamma) f_{\gamma_R}(\gamma)\,\mathrm{d}\gamma. \tag{2.16}$$

2.2 Analytical derivations

The analysis begins with the introduction of a single RIS system model presented in Figure 2.5, initially without considering practical phase shift model, using the Nakagami-m fading model to describe the signal propagation. Subsequently, the study advances to account for practical phase shift model, considering the case where $\kappa_{\min} = 0$ for the sake of simplicity of analytical derivation. To further refine the system model, the Fox-H function (see Appendix B) representation of the PDFs is employed, due to the fact that Fox-H functions can efficiently handle the process of finding the product of multiple identical random variables, which is essential for the analysis of cascaded RIS systems. This foundation sets the

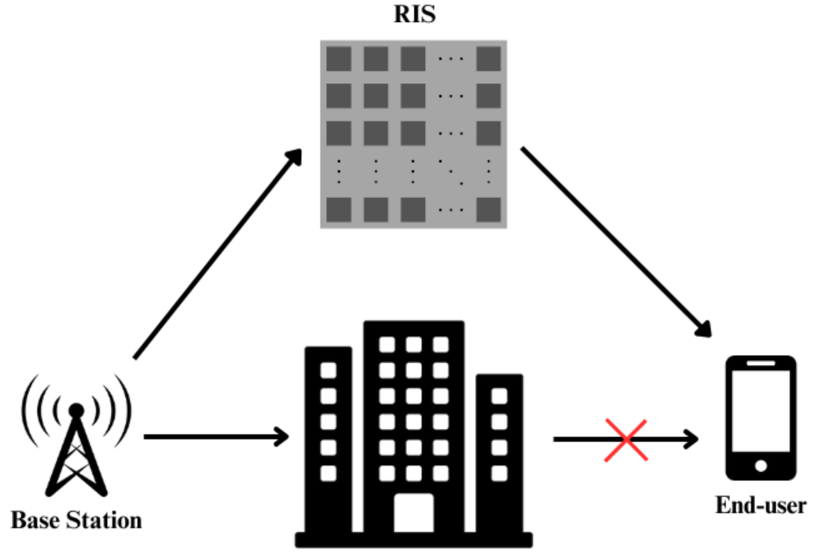

Figure 2.5: Single-RIS system model.

stage for the subsequent analysis of cascaded RIS systems, where multiple RIS elements are used in series.

2.2.1 Single RIS system model over Nakagami-m fading channel

A single RIS system model over a Nakagami-m fading channel is a scenario where an RIS is placed between the transmitter and receiver shown in Figure 2.5. Instantaneous end-to-end SNR of such system could be written as

$$\gamma_R = \frac{\left|\overline{P}\sum_{i=1}^{N} X_i e^{j\delta_i}\right|^2}{\sigma^2}, \tag{2.17}$$

where $\overline{P} = \sqrt{\frac{P}{d_{S-RIS}^T d_{RIS-R}^T}}$ is a normalized transmit power, $X_i = |h_i||v_i||q_i|$ is the product of amplitudes of random channels modeled by Nakagami-m distribution and reflection coefficient of RIS. In this section it is assumed that RIS is a perfect reflector, in other words, it's reflection coefficient is unity. Therefore, RIS only contributes to the signal by changing it's phase and phase of the received signal at the user side will be $\delta_i = \phi_i - \alpha_i + \psi_k$. For the sake of simplicity of analytical derivations, we assumed here that RIS fully compensate the channel phases, meaning that $\alpha_i = \phi_i + \psi_k$. Then, this problem simplifies to the finding the product of two Nakagami-m distribution and finding the sum of N such products. This can be formulated by creating a new random variable represented as Z

$$Z = \sum_{i=1}^{N} X_i = \sum_{i=1}^{N} |h_i||q_i|. \tag{2.18}$$

Now, the aim is to find the corresponding PDF and CDF of this new RV Z. First of all, the product of $|h_i||q_i|$ is needed. Here, both $|h_i|$ and $|q_i|$ are independent Nakagami-m RVs and can be represented by

$$f_{h_i}(a) = \frac{2m_{h_i}^{m_{h_i}}}{\Gamma(m_{h_i})\Omega_{h_i}^{m_{h_i}}} a^{2m_{h_i}-1} e^{-\frac{m_{h_i}}{\Omega_{h_i}}a^2}, \quad a \geq 0, \tag{2.19}$$

$$f_{q_i}(b) = \frac{2m_{q_i}^{m_{q_i}}}{\Gamma(m_{q_i})\Omega_{q_i}^{m_{q_i}}} b^{2m_{q_i}-1} e^{-\frac{m_{q_i}}{\Omega_{q_i}}b^2}, \quad b \geq 0. \tag{2.20}$$

Product of these independent and continuous two random variables can be found using the following rule

$$f_{X_i}(x) = \int_{-\infty}^{\infty} f_{h_i}(a) f_{q_i}\left(\frac{x}{a}\right) \frac{1}{|a|} \,\mathrm{d}a. \tag{2.21}$$

By substituting Nakagami-m distributions into this integral expression, we get

$$\begin{aligned} f_{X_i}(x) = \int_{-\infty}^{\infty} & \frac{2m_{h_i}^{m_{h_i}}}{\Gamma(m_{h_i})\Omega_{h_i}^{m_{h_i}}} a^{2m_{h_i}-1} e^{-\frac{m_{h_i}}{\Omega_{h_i}}a^2} \times \\ & \times \frac{2m_{q_i}^{m_{q_i}}}{\Gamma(m_{q_i})\Omega_{q_i}^{m_{q_i}}} \left(\frac{x}{a}\right)^{2m_{q_i}-1} e^{-\frac{m_{q_i}}{\Omega_{q_i}}\left(\frac{x}{a}\right)^2} \frac{1}{|a|} \,\mathrm{d}a. \end{aligned} \tag{2.22}$$

After some simplifying steps this expression transforms into

$$f_{X_i}(x) = \frac{2m_{h_i}^{m_{h_i}}}{\Gamma(m_{h_i})\Omega_{h_i}^{m_{h_i}}} \frac{2m_{q_i}^{m_{q_i}}}{\Gamma(m_{q_i})\Omega_{q_i}^{m_{q_i}}} x^{2m_{q_i}-1} \int_{0}^{\infty} a^{2m_{h_i}-2m_{q_i}-1} e^{-\frac{m_{h_i}}{\Omega_{h_i}}a^2 - \frac{m_{q_i}}{\Omega_{q_i}}\left(\frac{x}{a}\right)^2} \,\mathrm{d}a. \tag{2.23}$$

Applying the following substitution ($a^2 = t$) leads to

$$f_{X_i}(x) = \frac{2m_{h_i}^{m_{h_i}}}{\Gamma(m_{h_i})\Omega_{h_i}^{m_{h_i}}} \frac{2m_{q_i}^{m_{q_i}}}{\Gamma(m_{q_i})\Omega_{q_i}^{m_{q_i}}} \frac{1}{2} x^{2m_{q_i}-1} \int_{0}^{\infty} t^{m_{h_i}-m_{q_i}-1} e^{-\frac{m_{h_i}}{\Omega_{h_i}}t - \frac{m_{q_i}}{\Omega_{q_i}}\frac{x^2}{t}} \,\mathrm{d}t, \tag{2.24}$$

and it allows to use the identity from [29, Eq. (3.471.9)], which includes $K_\nu(\cdot)$ modified Bessel function of second kind

$$\int_0^\infty w^{\nu-1}e^{-\frac{\beta}{w}-\gamma w}\,\mathrm{d}w = 2\left(\frac{\beta}{\gamma}\right)^{\frac{\nu}{2}} K_\nu\left(2\sqrt{\beta\gamma}\right), \quad \operatorname{Re}\beta > 0, \operatorname{Re}\gamma > 0. \tag{2.25}$$

By noticing the similarity between this identity and integral in expression (2.24), and applying following substitutions $\nu = m_{h_i} - m_{q_i}, \beta = \frac{m_{q_i}}{\Omega_{q_i}}x^2, \gamma = \frac{m_{h_i}}{\Omega_{h_i}}$, resulting equation will be given by

$$\begin{aligned} f_{X_i}(x) = {} & \frac{2m_{h_i}^{m_{h_i}}}{\Gamma(m_{h_i})\Omega_{h_i}^{m_{h_i}}}\frac{2m_{q_i}^{m_{q_i}}}{\Gamma(m_{q_i})\Omega_{q_i}^{m_{q_i}}}\frac{1}{2}x^{2m_{q_i}-1}\times \\ & \times 2\left(\frac{\frac{m_{q_i}}{\Omega_{q_i}}x^2}{\frac{m_{h_i}}{\Omega_{h_i}}}\right)^{\frac{m_{h_i}-m_{q_i}}{2}} K_{m_{h_i}-m_{q_i}}\left(2\sqrt{\frac{m_{q_i}}{\Omega_{q_i}}x^2\frac{m_{h_i}}{\Omega_{h_i}}}\right). \end{aligned} \tag{2.26}$$

Upon simplification, the result is

$$f_{X_i}(x) = \frac{4}{\Gamma(m_{h_i})\Gamma(m_{q_i})}(\sqrt{\frac{m_{h_i}m_{q_i}}{\Omega_{h_i}\Omega_{q_i}}})^{m_{h_i}+m_{q_i}}x^{m_{h_i}+m_{q_i}-1}K_{m_{h_i}-m_{q_i}}\left(2x\sqrt{\frac{m_{h_i}m_{q_i}}{\Omega_{h_i}\Omega_{q_i}}}\right). \tag{2.27}$$

To further transform this expression, it is needed to employ the identity from [29, Eq. (9.34.3)]

$$K_\nu(w)w^\mu = 2^{\mu-1}G_{0,2}^{2,0}\left(\frac{1}{4}w^2\middle|\begin{matrix} - \\ \frac{1}{2}\mu+\frac{1}{2}\nu, \frac{1}{2}\mu-\frac{1}{2}\nu\end{matrix}\right). \tag{2.28}$$

This identity represents a relationship involving the modified Bessel function of the second kind $K_\nu(\cdot)$ and Meiger G-function (see Appendix A). Applying following substitutions $w = 2x\sqrt{\frac{m_{h_i}m_{q_i}}{\Omega_{h_i}\Omega_{q_i}}}, \nu = m_{h_i} - m_{q_i}, \mu = m_{h_i} + m_{q_i} - 1$ allow us to apply this identity on expression (2.27):

$$f_{X_i}(x) = \frac{2}{\Gamma(m_{h_i})\Gamma(m_{q_i})}\sqrt{\frac{m_{h_i}m_{q_i}}{\Omega_{h_i}\Omega_{q_i}}}G_{0,2}^{2,0}\left((\sqrt{\frac{m_{h_i}m_{q_i}}{\Omega_{h_i}\Omega_{q_i}}}x)^2\middle|\begin{matrix} - \\ m_{h_i}-\frac{1}{2}, m_{q_i}-\frac{1}{2}\end{matrix}\right). \tag{2.29}$$

This expression represents the product of two Nakagami-m RVs and expressed in terms of Meiger G-function. The next step is to find the sum of N such products, which defines a new RV Z. The sum of independent random variables is the convolution of their PDFs. Specifically, the PDF of Z is obtained by convolving the individual PDFs of RV presented in (2.29), resulting in a more complex distribution that accounts for the combined effects of the N Random Variables. The convolution of two RVs $Z = X + Y$ is performed by the following way

$$f_Z(z) = \int_{-\infty}^{\infty} f_X(x) f_Y(z - x)\,\mathrm{d}x. \tag{2.30}$$

Performing this operation N times is cumbersome, therefore, it is easier to perform this operation using Moment Generating Function (MGF), since it allows to find the sum by performing the multiplication of individual MGF's of each RV. The MGF of a random variable X is defined as [30]

$$M_X(t) = \mathbb{E}[e^{tX}]. \tag{2.31}$$

Having N independent random variables $X_1, X_2, \ldots, X_N$, MGF of the sum $Z = X_1 + X_2 + \cdots + X_N = \sum_{i=1}^{N} X_i$ is the product of the individual MGFs of each random variable

$$M_Z(z) = M_{X_1}(z) \cdot M_{X_2}(Z) \cdot \ldots \cdot M_{X_N}(z) = M_Z(z) = \prod_{i=1}^{N} M_{X_i}(z). \tag{2.32}$$

PDF of RV Z could be found by performing inverse MGF transform defined as

$$f_Z(z) = \mathcal{L}^{-1}\left[M_Z(z)\right](x). \tag{2.33}$$

At this point, it is needed to represent the expression (2.29) in terms of Fox H-function, since the derivation of PDF and CDF of sum of N RVs represented by Fox-H function is showed in [31]. This conversion process is performed using the following identity

$$H_{p,q}^{m,n}\left[z\left|\begin{smallmatrix}(a_1,C)(a_2,C)\cdots(a_p,C)\\(b_1,C)(b_2,C)\cdots(b_q,C)\end{smallmatrix}\right.\right] = \frac{1}{C} G_{p,q}^{m,n}\left(z^{1/C}\left|\begin{smallmatrix}a_1,\ldots,a_p\\b_1,\ldots,b_q\end{smallmatrix}\right.\right). \tag{2.34}$$

Then, the product of two Nakagami-m RVs can be presented using Fox-H functions as

$$f_{X_i}(x) = \frac{2}{\Gamma(m_{h_i})\Gamma(m_{q_i})}\sqrt{\frac{m_{h_i}m_{q_i}}{\Omega_{h_i}\Omega_{q_i}}}H^{2,0}_{0,2}\left[\left(\sqrt{\frac{m_{h_i}m_{q_i}}{\Omega_{h_i}\Omega_{q_i}}}x\right)^2 \middle| \begin{matrix} - \\ (m_{h_i}-\frac{1}{2},1),(m_{q_i}-\frac{1}{2},1)\end{matrix}\right]. \tag{2.35}$$

To do the procedure shown in [30], it is needed to have the PDF of a RV as

$$f_{X_i}(x) = \kappa_i H^{m_i,n_i}_{p_i,q_i}\left[\lambda_i x \middle| \begin{matrix} (a_{i,j},A_{i,j})_{j=1}^{p_i} \\ (b_{i,j},B_{i,j})_{j=1}^{q_i}\end{matrix}\right], \quad x > 0. \tag{2.36}$$

To transform the PDF in (2.35) in the showed format, it is needed to use Fox H-function property 1.4 from [32]:

$$H^{m,n}_{p,q}\left[z \middle| \begin{matrix} (a_p,A_p) \\ (b_q,B_q)\end{matrix}\right] = kH^{m,n}_{p,q}\left[z^k \middle| \begin{matrix} (a_p,kA_p) \\ (b_q,kB_q)\end{matrix}\right]. \tag{2.37}$$

Applying this property, (2.35) transforms into

$$f_{X_i}(x) = \frac{1}{\Gamma(m_{h_i})\Gamma(m_{q_i})}\sqrt{\frac{m_{h_i}m_{q_i}}{\Omega_{h_i}\Omega_{q_i}}}H^{2,0}_{0,2}\left[\sqrt{\frac{m_{h_i}m_{q_i}}{\Omega_{h_i}\Omega_{q_i}}}x \middle| \begin{matrix} - \\ (m_{h_i}-\frac{1}{2},\frac{1}{2}),(m_{q_i}-\frac{1}{2},\frac{1}{2})\end{matrix}\right]. \tag{2.38}$$

Then, according to [31], the PDF and CDF of a RV Z can be presented as

$$f_Z(z) = \frac{\prod_{i=1}^{N}\kappa_i\lambda_i^{-1}}{z}H^{0,0:m_1,n_1+1;\ldots;m_N,n_N+1}_{0,1:p_1+1,q_1;\ldots;p_N+1,q_N} \left[\begin{matrix}\lambda_1 z \\ \vdots \\ \lambda_N z\end{matrix} \middle| \begin{matrix} -:(1,1),(a_{1,j}+A_{1,j},A_{1,j})_{j=1}^{p_1};\ldots;(1,1)(a_{N,j}+A_{N,j},A_{N,j})_{j=1}^{p_N} \\ (1;1,\cdots,1):(b_{1,j}+B_{1,j},B_{1,j})_{j=1}^{q_1};\ldots;(b_{N,j}+B_{N,j},B_{N,j})_{j=1}^{q_N}\end{matrix}\right], \tag{2.39}$$

$$F_Z(z) = \prod_{i=1}^{N}\kappa_i\lambda_i^{-1}H^{0,0:m_1,n_1+1;\ldots;m_N,n_N+1}_{0,1:p_1+1,q_1;\ldots;p_N+1,q_N} \left[\begin{matrix}\lambda_1 z \\ \vdots \\ \lambda_N z\end{matrix} \middle| \begin{matrix} -:(1,1),(a_{1,j}+A_{1,j},A_{1,j})_{j=1}^{p_1};\ldots;(1,1)(a_{N,j}+A_{N,j},A_{N,j})_{j=1}^{p_N} \\ (1;1,\cdots,1):(b_{1,j}+B_{1,j},B_{1,j})_{j=1}^{q_1};\ldots;(b_{N,j}+B_{N,j},B_{N,j})_{j=1}^{q_N}\end{matrix}\right]. \tag{2.40}$$

Finally, using these results, it is possible to get the PDF and CDF of the sum of N products of Nakagami-m distribution as

$$f_Z(z) = \frac{1}{\Gamma(m_{h_i})\Gamma(m_{q_i})\cdots\Gamma(m_{h_N})\Gamma(m_{q_N})}\frac{1}{z}H^{0,0:2,1;\ldots;2,1}_{0,1:1,2;\ldots;1,2}\left[\begin{matrix}\sqrt{\frac{m_{h_1}m_{q_1}}{\Omega_{h_1}\Omega_{q_1}}}z\\ \vdots\\ \sqrt{\frac{m_{h_N}m_{q_N}}{\Omega_{h_N}\Omega_{q_N}}}z\end{matrix}\left|\begin{matrix}-:(1,1);\ldots;(1,1)\\ (1;1,\cdots,1):(m_{h_1},\frac{1}{2}),(m_{q_1},\frac{1}{2});\ldots(m_{h_N},\frac{1}{2}),(m_{q_N},\frac{1}{2})\end{matrix}\right.\right], \tag{2.41}$$

$$F_Z(z) = \frac{1}{\Gamma(m_{h_i})\Gamma(m_{q_i})\cdots\Gamma(m_{h_N})\Gamma(m_{q_N})}H^{0,0:2,1;\ldots;2,1}_{0,1:1,2;\ldots;1,2}\left[\begin{matrix}\sqrt{\frac{m_{h_1}m_{q_1}}{\Omega_{h_1}\Omega_{q_1}}}z\\ \vdots\\ \sqrt{\frac{m_{h_N}m_{q_N}}{\Omega_{h_N}\Omega_{q_N}}}z\end{matrix}\left|\begin{matrix}-:(1,1);\ldots;(1,1)\\ (1;1,\cdots,1):(m_{h_1},\frac{1}{2}),(m_{q_1},\frac{1}{2});\ldots(m_{h_N},\frac{1}{2}),(m_{q_N},\frac{1}{2})\end{matrix}\right.\right]. \tag{2.42}$$

Returning back to the instantaneous end-to-end SNR expression (2.17) and defining SNR as $\gamma_t = \overline{P}/\sigma^2$, we obtain

$$\gamma_R = \left|\sum_{i=1}^{N} X_i e^{j\delta_i}\right|^2 \gamma_t. \tag{2.43}$$

Rearranging it gives us the following form

$$\sum_{i=1}^{N} X_i e^{j\delta_i} = \sqrt{\frac{\gamma_R}{\gamma_t}}. \tag{2.44}$$

Using this form, it is possible to find the OP of this system as

$$P_{\text{out}} = \Pr\left(\sum_{i=1}^{N} X_i e^{j\delta_i} \leq \sqrt{\frac{\gamma_{\text{th}}}{\gamma_t}}\right) = F_Z\left(\sqrt{\frac{\gamma_{\text{th}}}{\gamma_t}}\right) \tag{2.45}$$

Then the exact OP expression of this system model could be expressed as

$$F_Z(\sqrt{\frac{\gamma_{\text{th}}}{\gamma_t}}) = \frac{1}{\Gamma(m_{h_i})\Gamma(m_{q_i})\cdots\Gamma(m_{h_N})\Gamma(m_{q_N})} H^{0,0:2,1;\ldots;2,1}_{0,1:1,2;\ldots;1,2} \left[\begin{matrix} \sqrt{\frac{m_{h_1}m_{q_1}}{\Omega_{h_1}\Omega_{q_1}}}\sqrt{\frac{\gamma_{\text{th}}}{\gamma_t}} \\ \vdots \\ \sqrt{\frac{m_{h_N}m_{q_N}}{\Omega_{h_N}\Omega_{q_N}}}\sqrt{\frac{\gamma_{\text{th}}}{\gamma_t}} \end{matrix} \middle| \begin{matrix} -:(1,1);\ldots;(1,1) \\ (0;1,\cdots,1):(m_{h_1},\frac{1}{2}),(m_{q_1},\frac{1}{2});\ldots(m_{h_N},\frac{1}{2}),(m_{q_N},\frac{1}{2}) \end{matrix} \right]. \tag{2.46}$$

In this section, finally, OP of the single RIS system model over Nakagami-m fading channel is derived considering RIS as a perfect reflector and assuming that it fully compensates the channel phases. In the following section practical RIS will be considered in the similar system model.

2.2.2 Derivation of the PDF of practical phase shift model

The aim of this section is to find the PDF in (2.8). It could be realized using the "change of RV" formula. In this section, it is still assumed that RIS fully compensates the channel phases as $\alpha_i = \phi_i + \psi_k$. We define a new RV $R \triangleq \rho_i(\alpha_i)$, where α_i is uniformly distributed between $-\pi$ and π ($\alpha_i \sim \mathcal{U}[-\pi, \pi]$). The first step is here is to solve for α_i in terms of r

$$\alpha_i = \vartheta + \arcsin\left(2\left(\frac{r - \kappa_{\min}}{1 - \kappa_{\min}}\right)^{1/\xi} - 1\right). \tag{2.47}$$

Then using the "change of RV" formula given by

$$f_{R_i} = f_\alpha(\alpha_i(r)) \cdot \left|\frac{\mathrm{d}\alpha_i}{\mathrm{d}r}\right|, \tag{2.48}$$

where $f_\alpha(\alpha_i)$ can be defined as

$$f_\alpha(\alpha_i) = \frac{1}{2\pi}, \tag{2.49}$$

and the derivative of α_i with respect to r is

$$\frac{\mathrm{d}\alpha_i}{\mathrm{d}r} = \frac{2}{\xi(1-\kappa_{\min})}\left(\frac{r-\kappa_{\min}}{1-\kappa_{\min}}\right)^{\frac{1}{\xi}-1} \times \frac{1}{\sqrt{1-\left(2\left(\frac{r-\kappa_{\min}}{1-\kappa_{\min}}\right)^{1/\xi}-1\right)^2}}. \tag{2.50}$$

Solving for the PDF of RV R gives

$$f_{R_i}(r) = \frac{1}{\pi\xi(1-\kappa_{\min})} \cdot \frac{\left(\frac{r-\kappa_{\min}}{1-\kappa_{\min}}\right)^{\frac{1}{\xi}-1}}{\sqrt{\left(\frac{r-\kappa_{\min}}{1-\kappa_{\min}}\right)^{1/\xi} - \left(\frac{r-\kappa_{\min}}{1-\kappa_{\min}}\right)^{2/\xi}}}, \quad r \in (\kappa_{\min}, 1]. \tag{2.51}$$

This PDF describes the distribution of the reflection amplitude $\rho_i(\alpha_i)$ in a RIS, where the amplitude depends nonlinearly on the reflection phase α_i. Assuming α_i is uniformly distributed, this function models how random phase shifts translate into specific amplitude variations, capturing practical RIS behavior with shaping parameter ξ and minimum reflection level $\kappa_{\min}$.

2.2.3 Single-RIS system model over Nakagami-m fading channel with a practical phase shift model

In this section, the practical phase shift model will be applied to the system model, and following notation will be used for SNR:

$$\gamma_R = \frac{\left|\overline{P}\sum_{i=1}^{N} Y_i e^{j\delta_i}\right|^2}{\sigma^2}, \tag{2.52}$$

where $Y_i = |h_i||v_i||q_i|$ is the product of channel gains with reflection coefficients as a function of phase shift. Other notations are same as in the previous sections. Due to the complexity of the PDF in (2.51), setting $\kappa_{\min}$ to zero allows us to compute OP. By setting $\kappa_{\min} = 0$, the PDF expression in (2.51) simplifies into

$$f_R(r) = \frac{1}{\pi\xi} \cdot \frac{(r)^{\frac{1}{\xi}-1}}{\sqrt{(r)^{1/\xi} - (r)^{2/\xi}}}, \quad r \in (0, 1]. \tag{2.53}$$

In this equation, it is assumed that all reflective elements have similar parameters ξ, therefore subscripts for this expression are omitted. PDF for the product of two Nakagami-m RVs was already defined in expression (2.38). Now, we will define a new RV $Y \triangleq XR$, and it's PDF will derived using product of two RV formula

$$f_{Y_i}(y) = \int_{-\infty}^{\infty} f_{X_i}(x) f_{R_i}\left(\frac{y}{x}\right) \frac{1}{|x|}\, \mathrm{d}x. \tag{2.54}$$

Substituting the distributions accordingly, we get

$$\begin{aligned} f_{Y_i}(y) = {} & \frac{1}{\pi\xi} \frac{1}{\Gamma(m_{h_i})\Gamma(m_{q_i})} \sqrt{\frac{m_{h_i} m_{q_i}}{\Omega_{h_i}\Omega_{q_i}}} \times \\ & \times \int_{y}^{\infty} H_{0,2}^{2,0}\left[\sqrt{\frac{m_{h_i} m_{q_i}}{\Omega_{h_i}\Omega_{q_i}}} x \,\middle|\, \begin{matrix} - \\ (m_{h_i}-\frac{1}{2},\frac{1}{2}),(m_{q_i}-\frac{1}{2},\frac{1}{2}) \end{matrix} \right] \cdot \frac{\left(\frac{y}{x}\right)^{\frac{1}{\xi}-1}}{\sqrt{\left(\frac{y}{x}\right)^{1/\xi} - \left(\frac{y}{x}\right)^{2/\xi}}} \frac{1}{x}\, \mathrm{d}x. \end{aligned} \tag{2.55}$$

By making the following variable change $u = (\frac{y}{x})^{\frac{1}{\xi}}$, the following transfomrations will happen $x = \frac{y}{u^{\xi}}$, $dx = \frac{-\xi y}{u^{\xi+1}} du$, and the bounds of integral will be from 1 to 0, however, since there is a minus sign, these integral bound become from 0 to 1 as

$$\begin{aligned} f_{Y_i}(y) = {} & \frac{1}{\pi\xi} \frac{1}{\Gamma(m_{h_i})\Gamma(m_{q_i})} \sqrt{\frac{m_{h_i} m_{q_i}}{\Omega_{h_i}\Omega_{q_i}}} \times \\ & \times \int_{0}^{1} H_{0,2}^{2,0}\left[\sqrt{\frac{m_{h_i} m_{q_i}}{\Omega_{h_i}\Omega_{q_i}}} \frac{y}{u^{\xi}} \,\middle|\, \begin{matrix} - \\ (m_{h_i}-\frac{1}{2},\frac{1}{2}),(m_{q_i}-\frac{1}{2},\frac{1}{2}) \end{matrix} \right] \cdot \frac{u^{1-\xi}}{\sqrt{u-u^2}} \frac{u^{\xi}}{y} \frac{\xi y}{u^{\xi+1}}\, \mathrm{d}u. \end{aligned} \tag{2.56}$$

After simplifying the last expression, it transforms into

$$\begin{aligned} f_{Y_i}(y) = {} & \frac{1}{\pi} \frac{1}{\Gamma(m_{h_i})\Gamma(m_{q_i})} \sqrt{\frac{m_{h_i} m_{q_i}}{\Omega_{h_i}\Omega_{q_i}}} \times \\ & \times \int_{0}^{1} H_{0,2}^{2,0}\left[\sqrt{\frac{m_{h_i} m_{q_i}}{\Omega_{h_i}\Omega_{q_i}}} \frac{y}{u^{\xi}} \,\middle|\, \begin{matrix} - \\ (m_{h_i}-\frac{1}{2},\frac{1}{2}),(m_{q_i}-\frac{1}{2},\frac{1}{2}) \end{matrix} \right] \cdot \frac{1}{\sqrt{u-u^2}} \frac{1}{u^{\xi}}\, \mathrm{d}u. \end{aligned} \tag{2.57}$$

Now, it is needed to employ the definition of Fox H-function and expand the latter inside the integral. The expansion will be performed as follows

$$H_{0,2}^{2,0}\left[\sqrt{\frac{m_{h_i}m_{q_i}}{\Omega_{h_i}\Omega_{q_i}}}\cdot\frac{y}{u^{\xi}}\;\middle|\;\begin{matrix} - \\ \left(m_{h_i}-\frac{1}{2},\frac{1}{2}\right),\ \left(m_{q_i}-\frac{1}{2},\frac{1}{2}\right)\end{matrix}\right]= \\ \frac{1}{2\pi i}\int_L \Gamma\left(m_{h_i}-\frac{1}{2}+\frac{1}{2}s\right)\Gamma\left(m_{q_i}-\frac{1}{2}+\frac{1}{2}s\right)\left(\sqrt{\frac{m_{h_i}m_{q_i}}{\Omega_{h_i}\Omega_{q_i}}}\cdot\frac{y}{u^{\xi}}\right)^{-s}\mathrm{d}s. \tag{2.58}$$

Putting this expanded version of Fox H-function, we obtain

$$\begin{aligned} f_{Y_i}(y)=\frac{1}{\pi}\frac{1}{\Gamma(m_{h_i})\Gamma(m_{q_i})}\sqrt{\frac{m_{h_i}m_{q_i}}{\Omega_{h_i}\Omega_{q_i}}}\int_0^1\frac{1}{2\pi i}\int_L\Gamma\left(m_{h_i}-\frac{1}{2}+\frac{1}{2}s\right)\times \\ \times\Gamma\left(m_{q_i}-\frac{1}{2}+\frac{1}{2}s\right)\left(\sqrt{\frac{m_{h_i}m_{q_i}}{\Omega_{h_i}\Omega_{q_i}}}\frac{y}{u^{\xi}}\right)^{-s}ds\frac{1}{\sqrt{u-u^2}}\frac{1}{u^{\xi}}\,\mathrm{d}u. \end{aligned} \tag{2.59}$$

After rearranging the terms, the last expression transforms into

$$\begin{aligned} f_{Y_i}(y)=\frac{1}{\pi}\frac{1}{\Gamma(m_{h_i})\Gamma(m_{q_i})}\sqrt{\frac{m_{h_i}m_{q_i}}{\Omega_{h_i}\Omega_{q_i}}}\frac{1}{2\pi i}\int_L\Gamma\left(m_{h_i}-\frac{1}{2}+\frac{1}{2}s\right)\times \\ \times\Gamma\left(m_{q_i}-\frac{1}{2}+\frac{1}{2}s\right)\left(\sqrt{\frac{m_{h_i}m_{q_i}}{\Omega_{h_i}\Omega_{q_i}}}y\right)^{-s}ds\int_0^1 u^{\xi s-\xi-\frac{1}{2}}(1-u^2)^{-\frac{1}{2}}\,\mathrm{d}u. \end{aligned} \tag{2.60}$$

In order to solve the latter integral, Beta function [33] could be employed, it is defined as

$$B(a,b)=\int_0^1 t^{a-1}(1-t)^{b-1}\,dt=\frac{\Gamma(a)\Gamma(b)}{\Gamma(a+b)},\quad \text{for } a>0,b>0. \tag{2.61}$$

Using the definition of Beta function to solve the integral in (2.60) will result in

$$\int_0^1 u^{\xi s-\xi-\frac{1}{2}}(1-u^2)^{-\frac{1}{2}}\,\mathrm{d}u=\frac{\Gamma(\frac{1}{2}-\xi+\xi s)\Gamma(\frac{1}{2})}{\Gamma(1-\xi+\xi s)}. \tag{2.62}$$

Let's substitute this result into expression (2.60), and using $\Gamma(\frac{1}{2}) = \sqrt{\pi}$, we obtain

$$
\begin{aligned}
f_{Y_i}(y) = {}& \frac{1}{\sqrt{\pi}} \frac{1}{\Gamma(m_{h_i})\Gamma(m_{q_i})} \sqrt{\frac{m_{h_i} m_{q_i}}{\Omega_{h_i}\Omega_{q_i}}} \times \\
&\times \frac{1}{2\pi i} \int_L \frac{\Gamma(\frac{1}{2} - \xi + \xi s)\Gamma\left(m_{h_i} - \frac{1}{2} + \frac{1}{2}s\right)\Gamma\left(m_{q_i} - \frac{1}{2} + \frac{1}{2}s\right)}{\Gamma(1 - \xi + \xi s)} \left(\sqrt{\frac{m_{h_i} m_{q_i}}{\Omega_{h_i}\Omega_{q_i}}} y\right)^{-s} \mathrm{d}s.
\end{aligned} \tag{2.63}
$$

Relying on the definition of the Fox H-function, it is possible to rewrite the last expression in terms of H-function [32]. Then, the final expression will look

$$
f_{Y_i}(y) = \frac{1}{\sqrt{\pi}} \frac{1}{\Gamma(m_{h_i})\Gamma(m_{q_i})} \sqrt{\frac{m_{h_i} m_{q_i}}{\Omega_{h_i}\Omega_{q_i}}} H^{3,0}_{1,3}\left[\sqrt{\frac{m_{h_i} m_{q_i}}{\Omega_{h_i}\Omega_{q_i}}} y \,\middle|\, \begin{matrix} (1-\xi,\xi) \\ (m_{h_i}-\frac{1}{2},\frac{1}{2}),(m_{q_i}-\frac{1}{2},\frac{1}{2}),(\frac{1}{2}-\xi,\xi) \end{matrix} \right]. \tag{2.64}
$$

Repeating the same procedure as in (2.39) and (2.40), the PDF and CDF of sum of N such products can be obtained as $Z = \sum_{i=1}^{N} Y_i$

$$
\begin{aligned}
f_Z(z) = {}& \frac{1}{\sqrt{\pi}} \frac{1}{\Gamma(m_{h_i})\Gamma(m_{q_i}) \cdots \Gamma(m_{h_N})\Gamma(m_{q_N})} \frac{1}{z} H^{0,0:3,1;\ldots;3,1}_{0,1:2,3;\ldots;2,3} \\
& \left[\begin{matrix} \sqrt{\frac{m_{h_1} m_{q_1}}{\Omega_{h_1}\Omega_{q_1}}} z \\ \vdots \\ \sqrt{\frac{m_{h_N} m_{q_N}}{\Omega_{h_N}\Omega_{q_N}}} z \end{matrix} \,\middle|\, \begin{matrix} -:(1,1),(1-\xi,\xi);\ldots;(1,1),(1-\xi,\xi) \\ (0;1,\cdots,1):(m_{h_1},\frac{1}{2}),(m_{q_1},\frac{1}{2}),(\frac{1}{2}-\xi,\xi);\ldots(m_{h_N},\frac{1}{2}),(m_{q_N},\frac{1}{2}),(\frac{1}{2}-\xi,\xi) \end{matrix} \right],
\end{aligned} \tag{2.65}
$$

$$
\begin{aligned}
F_Z(z) = {}& \frac{1}{\sqrt{\pi}} \frac{1}{\Gamma(m_{h_i})\Gamma(m_{q_i}) \cdots \Gamma(m_{h_N})\Gamma(m_{q_N})} H^{0,0:3,1;\ldots;3,1}_{0,1:2,3;\ldots;2,3} \\
& \left[\begin{matrix} \sqrt{\frac{m_{h_1} m_{q_1}}{\Omega_{h_1}\Omega_{q_1}}} z \\ \vdots \\ \sqrt{\frac{m_{h_N} m_{q_N}}{\Omega_{h_N}\Omega_{q_N}}} z \end{matrix} \,\middle|\, \begin{matrix} -:(1,1),(1-\xi,\xi);\ldots;(1,1),(1-\xi,\xi) \\ (0;1,\cdots,1):(m_{h_1},\frac{1}{2}),(m_{q_1},\frac{1}{2}),(\frac{1}{2}-\xi,\xi);\ldots(m_{h_N},\frac{1}{2}),(m_{q_N},\frac{1}{2}),(\frac{1}{2}-\xi,\xi) \end{matrix} \right].
\end{aligned} \tag{2.66}
$$

Using this CDF, it is possible to find the OP as follows

$$
P_{\text{out}} = \Pr\left(\sum_{i=1}^{N} Y_i e^{j\delta_i} \leq \sqrt{\frac{\gamma_{\text{th}}}{\gamma_t}} \right) = F_Z\left(\sqrt{\frac{\gamma_{\text{th}}}{\gamma_t}} \right) \tag{2.67}
$$

Then, the OP for this system model can be found as

$$F_Z(\sqrt{\frac{\gamma_{\text{th}}}{\gamma_t}}) = \frac{1}{\sqrt{\pi}}\frac{1}{\Gamma(m_{h_i})\Gamma(m_{q_i})\cdots\Gamma(m_{h_N})\Gamma(m_{q_N})} H^{0,0:3,1;\ldots;3,1}_{0,1:2,3;\ldots;2,3} \left[\begin{matrix} \sqrt{\frac{m_{h_1}m_{q_1}}{\Omega_{h_1}\Omega_{q_1}}}\sqrt{\frac{\gamma_{\text{th}}}{\gamma_t}} \\ \vdots \\ \sqrt{\frac{m_{h_N}m_{q_N}}{\Omega_{h_N}\Omega_{q_N}}}\sqrt{\frac{\gamma_{\text{th}}}{\gamma_t}} \end{matrix}\middle| \begin{matrix} -:(1,1),(1-\xi,\xi);\ldots;(1,1),(1-\xi,\xi) \\ (0;1,\cdots,1):(m_{h_1},\frac{1}{2}),(m_{q_1},\frac{1}{2}),(\frac{1}{2}-\xi,\xi);\ldots(m_{h_N},\frac{1}{2}),(m_{q_N},\frac{1}{2}),(\frac{1}{2}-\xi,\xi) \end{matrix}\right]. \tag{2.68}$$

2.2.4 Fox H-function implementation for RIS-based communication

Multiplicative property of Mellin Tranform

The multiplicative property of the Mellin transform has significant potential for applications in the context RIS. In the case of cascaded RIS systems, this property can be leveraged to simplify the analysis and find the product of several RVs. Mellin Transform for a non-negative RV Y is defined as [28]

$$\mathcal{M}_Y(s) = \mathbb{E}[Y^{s-1}] = \int_0^\infty y^{s-1} f_Y(y)\,\mathrm{d}y, \tag{2.69}$$

where s is a complex variable, and $f_Y(y)$ is PDF of the RV Y. Let us now consider multiple independent non-negative RVs Y_1, Y_2, $\cdots$, Y_n. The product of two RVs could be found using the following formula, where a new random variable is identified as a product of two RVs $Z = Y_i Y_j$ as [34]

$$f_Z(z) = \int_{-\infty}^{\infty} f_{Y_i}(y_i) f_{Y_j}\left(\frac{z}{y_i}\right)\frac{1}{|y_i|}\,\mathrm{d}y_i. \tag{2.70}$$

In order to find the product of multiple RVs, it is required to use formula above iteratively, which is complex. Therefore, using the multiplicative property of Mellin Transform will simplify this process. Suppose that product of RVs Y_1, Y_2, $\cdots$, Y_n

is Z as follows

$$Z = \prod_{k=1}^{n} Y_k. \tag{2.71}$$

Then, the Mellin Transform of Z is the multiplication of individual Mellin Transforms of each random variable Y_1, Y_2, $\cdots$, Y_n [35]:

$$\mathcal{M}_Z(s) = \mathbb{E}\left[Z^{s-1}\right] = \prod_{k=1}^{n} \mathcal{M}_{Y_k}(s). \tag{2.72}$$

Next step is to take the inverse Mellin Transform of RV Z. Inverse Mellin Transform for random variable Z is defined as [35]

$$f_Z(z) = \mathcal{M}_z^{-1}\{\mathcal{M}_z(s)\} = \frac{1}{2\pi i}\int_{c-i\infty}^{c+i\infty} \mathcal{M}_z(s) z^{-s}\,\mathrm{d}s. \tag{2.73}$$

Using this approach, it is possible to find the distribution of the product of channel gains and reflection coefficients. This requires to finding the individual Mellin Transforms of the Nakagami-m distribution and the distribution of amplitude response of practical phase shift.

Mellin Transform and Fox-H representation of Nakagami-m Distribution

The PDF of Nakagami-m distribution is presented in (2.4). Its Mellin Transform was found using the integration by substitution and definition of Gamma function:

$$\mathcal{M}_{f_{X_i}}(s) = \left(\frac{m_i}{\Omega_i}\right)^{\frac{1-s}{2}} \frac{\Gamma\left(\frac{s+2m_i-1}{2}\right)}{\Gamma(m_i)} \tag{2.74}$$

By taking inverse Mellin Transform, we get

$$f_{X_i}(x) = \sqrt{\frac{m_i}{\Omega_i}} \cdot \frac{1}{\Gamma(m_i)} \cdot \frac{1}{2\pi i}\int_{L_i} \left(x\sqrt{\frac{m_i}{\Omega_i}}\right)^{-s} \Gamma\left(\frac{s+2m_i-1}{2}\right) \mathrm{d}s. \tag{2.75}$$

Eventually, Nakagami-m could be presented in the form of Fox H-function, since it is written using Mellin-Barnes type integral

$$f_{X_i}(x) = \sqrt{\frac{m_i}{\Omega_i}} \cdot \frac{1}{\Gamma(m_i)} H_{0,1}^{1,0} \left[\sqrt{\frac{m_i}{\Omega_i}} x \,\middle|\, \begin{matrix} - \\ (m_i - \frac{1}{2}, \frac{1}{2}) \end{matrix} \right]. \tag{2.76}$$

Due to the multiplicative property of Mellin Transforms, it is possible to find the product of several Nakagami-m RVs, so the general formula for the product of N such RVs ($Z = \prod_{i=1}^{N} X_i$) will be

$$\begin{aligned} f_Z(z) = \sqrt{\frac{m_1 \dots m_N}{\Omega_1 \dots \Omega_N}} \cdot \frac{1}{\Gamma(m_1) \dots \Gamma(m_N)} H_{0,N}^{N,0} \\ \left[\sqrt{\frac{m_1 \dots m_N}{\Omega_1 \dots \Omega_N}} z \,\middle|\, \begin{matrix} - \\ (m_1 - \frac{1}{2}, \frac{1}{2}) \dots (m_N - \frac{1}{2}, \frac{1}{2}) \end{matrix} \right]. \end{aligned} \tag{2.77}$$

Mellin Transform and Fox-H representation of Amplitude Response of Practical Phase Shift

The same procedure could be made on function of amplitude response on phase shift, which represented in (1.3). Defining $R_i^{R_t} \triangleq \rho_i^{R_t}(\alpha_i^{R_t})$, the distribution of amplitude response could be found as [21]

$$f_{R^{R_t}}(r) = \frac{\left(\frac{r-\kappa_{\min}}{1-\kappa_{\min}}\right)^{1/\xi-1}}{\pi\xi(1-\kappa_{\min})\sqrt{\left(\frac{r-\kappa_{\min}}{1-\kappa_{\min}}\right)^{1/\xi} - \left(\frac{r-\kappa_{\min}}{1-\kappa_{\min}}\right)^{2/\xi}}}. \tag{2.78}$$

Mellin Transform of such distribution is complex, therefore to simplify analytical derivations, $\kappa_{\min}$ was set to 0. Further derivations included integration by substitution and usage of Beta function [36], which led to

$$M_{f_{R^{R_t}}}(s) = \frac{1}{\sqrt{\pi}} \cdot \frac{\Gamma(\xi s - \xi + \frac{1}{2})}{\Gamma(\xi s - \xi + 1)}. \tag{2.79}$$

Here, again it is assumed that all reflective elemets have same circuit parameters, therefore subscripts indicating the i-th elements are omitted. Taking the inverse

Mellin Trasform, similarity with Mellin-Barnes type integral could be noticed, and amplitude response could be represented using Fox H-function [37] as

$$f_{R^{R_t}}(r) = \frac{1}{\sqrt{\pi}} H_{1,0}^{1,1}\left[r \,\middle|\, \begin{matrix} (-\xi+1,\xi) \\ (\frac{1}{2}-\xi,\xi) \end{matrix} \right]. \tag{2.80}$$

Similarly, using the multiplicative property of Mellin Transform, this expression can be extended as a product of N such distributions ($Z = \prod_{i=1}^{N} R_i$)

$$f_Z(z) = \left(\frac{1}{\sqrt{\pi}}\right)^N H_{N,0}^{N,N}\left[z \,\middle|\, \begin{matrix} (-\xi+1,\xi)\dots(-\xi+1,\xi) \\ (\frac{1}{2}-\xi,\xi)\dots(\frac{1}{2}-\xi,\xi) \end{matrix} \right]. \tag{2.81}$$

2.2.5 Analysis of cascaded RIS system model

In cascaded RIS system model, the main focus will be devoted to the SNR expression presented in (2.9). Firstly, another view towards the sums will be introduced, then product of channel gains and reflection coefficients will be derived, and, finally, potential solution for addressing phase errors will be presented in.

Alternative view on the sums in the cascaded RIS system model

In this section, a new method for representing several sums in SNR expression with a single sum will be presented. It can be noticed that the sums in SNR are not nested summations, these summations aims to find the sums of products of channel gains and reflection coefficients for each path between the transmitter and receiver. For example, consider Figure 2.2, where 64 paths exist between the the transmitter and receiver. These path can be viewed as a product of corresponding channel gains and reflection coefficients, and summations in SNR expression finds the sum of all these products. The general idea is presented by the expression below:

$$\sum_{i=1}^{N}\sum_{l=1}^{N}\cdots\sum_{j=1}^{N}\sum_{k=1}^{N} X_{il\cdots jk} = \sum_{m=1}^{N^d} X_m, \tag{2.82}$$

where m (path index) is connected to the other indices by the following expression:

$$m = (i-1)N^{d-1} + (j-1)N^{d-2} + \cdots + (k-1)N + (l-1) + 1. \tag{2.83}$$

Here, d depends on how many summations there are, in other words, it is the number of RISs in the system model. Returning again to the example in Figure 2.2, there are three RISs each with four reflecting elements. Here, m will be any number between the 1 and $4^3 = 64$ showing the index number of the particular path. Knowing the index number of any path, it is possible to derive the indices from the original SNR expression:

$$i = \lfloor \frac{m-1}{N^{d-1}} \rfloor + 1, \tag{2.84}$$

$$j = \lfloor \frac{(m-1) \mod N^{d-1}}{N^{d-2}} \rfloor + 1, \tag{2.85}$$

$$\vdots$$

$$k = \lfloor \frac{(m-1) \mod N^{2}}{N} \rfloor + 1, \tag{2.86}$$

$$l = \lfloor (m-1) \mod N \rfloor + 1. \tag{2.87}$$

It is possible to generalize these expression using the following indices i_1, i_2, $\cdots$, i_p, $\cdots$, i_d, then

$$m = \sum_{p=1}^{d} (i_p - 1)N^{d-p} + 1, \tag{2.88}$$

$$i_p = \lfloor \frac{(m-1) \mod N^{d-p+1}}{N^{d-p}} \rfloor + 1. \tag{2.89}$$

This alternative view towards the summation in the SNR expression simplifies the representation of the path index, making it easier to analyze and optimize the cascaded RIS model by reducing the complexity of nested summations.

Suggested approach for addressing phase errors in the cascaded RIS system

It was already stated that phase errors are inherent in cascaded RIS system model. However, at this stage, it is roughly assumed that RIS phases fully compensates the random channel phases, which is impossible in reality. Even though, the idea dealing with these phase errors will be presented in this paper. Phase errors in SNR expression can be addressed with the utilization of Euler's formula, which establishes the relationship between the trigonometric functions and the complex exponential function as

$$e^{ix} = \cos x + i \sin x. \tag{2.90}$$

These trigonometric function in Euler's identity can be further represented by special functions. Below Meiger G-function representations are shown:

$$\cos x = \sqrt{\pi} G_{0,2}^{1,0}\left(\frac{x^2}{4} \middle|_{0,\frac{1}{2}}^{-} \right), \quad \forall x, \tag{2.91}$$

$$\sin x = \sqrt{\pi} G_{0,2}^{1,0}\left(\frac{x^2}{4} \middle|_{\frac{1}{2},0}^{-} \right), \quad \frac{-\pi}{2} < \arg x \leq \frac{\pi}{2}. \tag{2.92}$$

Derivation of products of channel gains and reflection coefficients

For the cascaded RIS-based system model presented in Figure 2.1, the approach finding the product of channel gain and reflection coefficients are similar as for single RIS sytem model. It is accomplished by the utilization of product of two RVs formula, where we multiply the RVs presented in expressions 2.77 and 2.81. In cascaded RIS system model, one path is consists of $N + 1$ random channels, where N is the number of RIS in series. Therefore, two random variable that are going to be multiplied could be written as

$$f_{Z_i}(z) = \sqrt{\frac{m_{i,1}\dots m_{i,N}, m_{i,N+1}}{\Omega_{i,1}\dots\Omega_{i,N}, \Omega_{i,N+1}}} \cdot \frac{1}{\Gamma(m_{i,1})\dots\Gamma(m_{i,N})\Gamma(m_{i,N+1})} H^{N+1,0}_{0,N+1} \left[\sqrt{\frac{m_{i,1}\dots m_{i,N}, m_{i,N+1}}{\Omega_{i,1}\dots\Omega_{i,N},, \Omega_{i,N+1}}} z \,\middle|\, \begin{matrix} - \\ (m_{i,1}-\frac{1}{2},\frac{1}{2})\dots(m_{i,N}-\frac{1}{2},\frac{1}{2}),(m_{i,N+1}-\frac{1}{2},\frac{1}{2}) \end{matrix} \right], \tag{2.93}$$

$$f_{T_i}(t) = (\frac{1}{\sqrt{\pi}})^N H^{N,N}_{N,0} \left[t \,\middle|\, \begin{matrix} (-\xi_{i,1}+1,\xi_{i,1})\dots(-\xi_{i,N}+1,\xi_{i,N}) \\ (\frac{1}{2}-\xi_{i,1},\xi_{i,1})\dots(\frac{1}{2}-\xi_{i,N},\xi_{i,N}) \end{matrix} \right], \tag{2.94}$$

where i is the index of the particular path. In the latter expression it is assumed that all the reflecting elements in all RISs are identical, therefore, all these elements have the same value of ξ and $\kappa_{\min} = 0$, despite the indexation done. Then the product of the RVs can be written as:

$$f_{V_i}(v) = \int_{-\infty}^{\infty} f_{Z_i}(z) f_{T_i}\left(\frac{v}{z}\right) \frac{1}{|z|}\,\mathrm{d}z. \tag{2.95}$$

Substituting into the product formula, we obtain:

$$f_{V_i}(v) = (\frac{1}{\sqrt{\pi}})^N \sqrt{\frac{m_{i,1}\dots m_{i,N}, m_{i,N+1}}{\Omega_{i,1}\dots\Omega_{i,N}, \Omega_{i,N+1}}} \frac{1}{\Gamma(m_{i,1})\dots\Gamma(m_{i,N})\Gamma(m_{i,N+1})} \int_{-\infty}^{\infty} H^{N+1,0}_{0,N+1} \left[\sqrt{\frac{m_{i,1}\dots m_{i,N}, m_{i,N+1}}{\Omega_{i,1}\dots\Omega_{i,N},, \Omega_{i,N+1}}} z \,\middle|\, \begin{matrix} - \\ (m_{i,1}-\frac{1}{2},\frac{1}{2})\dots(m_{i,N}-\frac{1}{2},\frac{1}{2}),(m_{i,N+1}-\frac{1}{2},\frac{1}{2}) \end{matrix} \right] \times \\ \times H^{N,N}_{N,0} \left[\frac{v}{z} \,\middle|\, \begin{matrix} (-\xi_{i,1}+1,\xi_{i,1})\dots(-\xi_{i,N}+1,\xi_{i,N}) \\ (\frac{1}{2}-\xi_{i,1},\xi_{i,1})\dots(\frac{1}{2}-\xi_{i,N},\xi_{i,N}) \end{matrix} \right] \frac{1}{|z|}\,\mathrm{d}z. \tag{2.96}$$

This section is still in progress due to the complexity of deriving the product of channel gains and reflection coefficients in the cascaded RIS system.

Challenges of correlated summations in cascaded RIS systems

In a cascaded RIS system model, the paths are not independent, and instead, they exhibit varying degrees of correlation between each other. These correlations arise due to the common environment and shared elements between the transmitter, RIS, and receiver, which can result in interdependencies that complicate the mathematical treatment of the system. Due to the complexity of these correlations, accurately modeling has not yet been fully accomplished, as assuming independence can lead to inaccurate results.

Chapter 3

Results

This chapter presents the key findings from the analysis and simulations conducted on RIS-based communication systems. The results are organized into two subsections, each corresponding to specific models and their respective performance metrics. Firstly, the performance of a single RIS system model is analyzed under the assumption of both ideal and practical phase shift conditions, with a focus on the OP for varying numbers of reflecting elements and threshold values. The results of these analyses are compared against the derived analytical expressions to validate the accuracy of the model. Secondly, the simulation results for the cascaded RIS system model are presented. These simulations examine the performance metrics of OP and EC, both with and without phase errors. The results are presented through various graphs, illustrating the effects of phase errors on system performance across different configurations of RIS elements and RIS layers.

3.1 Single RIS system model over Nakagami-m fading channel

In this section, we present the results for the single RIS system model over a Nakagami-m fading channel, considering both the case with and without the practical phase shift model. The analysis focuses on the OP, which is a key performance metric in wireless communication systems. To evaluate the system's performance, we use Monte Carlo simulations with one million samples. For the following graphs presented in Figure 3.1 and 3.2, Nakagami-m parameters taken as unity ($m_{h_i} = 1, m_{q_i} = 1, \Omega_{h_i} = 1, \Omega_{q_i} = 1, \quad \forall i$), where i is the number of

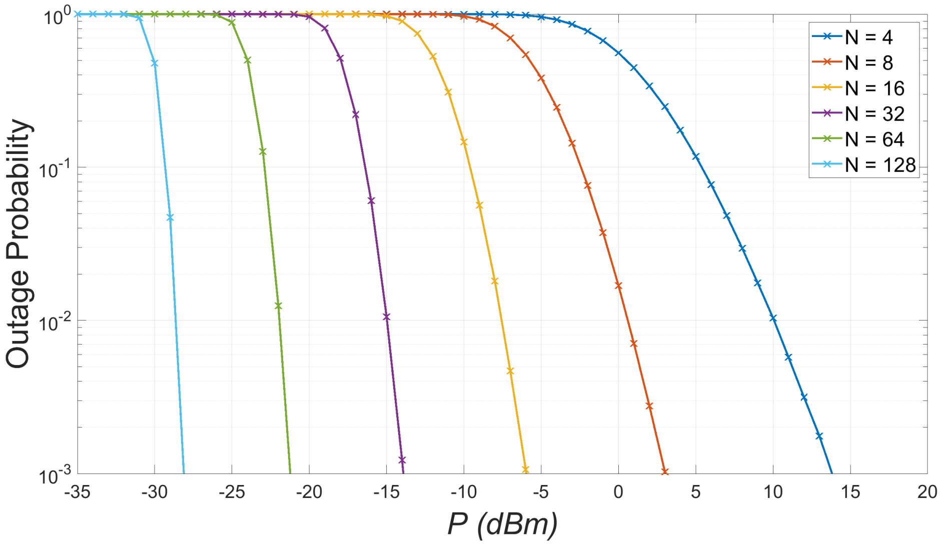

Figure 3.1: OP for a single RIS system model over a Nakagami-m fading channel without the practical phase shift model. The OP is plotted for varying numbers of reflecting elements.

reflecting elements. Analytical expression for this case shown in (2.46) involves multivariate Fox H-function, and its numerical implementation in Python programming language is presented in [38].

Figure 3.1 illustrates the OP of the single RIS system model over a Nakagami-m fading channel without the practical phase shift model, where the number of reflecting elements is varied. In this case, threshold value is set to 10. From this figure, we observe that as the number of reflecting elements increases, the OP decreases, demonstrating that a larger RIS array enhances the system's reliability. This trend highlights the positive impact of increasing the number of reflecting elements, as it allows for better signal enhancement.

Figure 3.2 shows the OP for various threshold values, while the number of reflecting elements is fixed to 16. Here, we see that as the threshold increases, the OP also rises. This suggests that higher thresholds reduce the acceptable signal range, thereby increasing the likelihood of an outage. This result is expected, as the system becomes more sensitive to signal strength when the threshold is set higher.

Notably, the results from both graphs are in perfect alignment with the an-

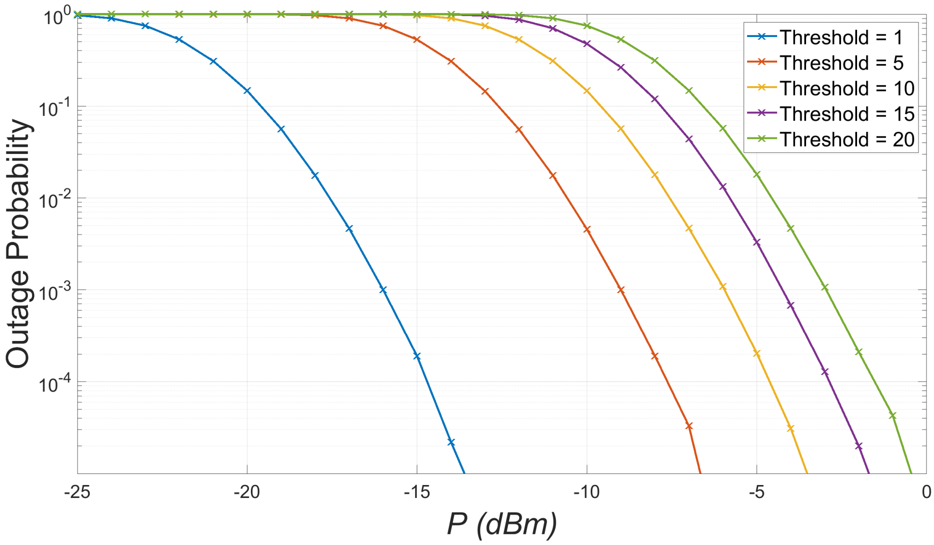

Figure 3.2: OP for a single RIS system model over a Nakagami-m fading channel without the practical phase shift model. The OP is plotted for varying threshold values.

alytical expressions derived earlier. The agreement between the Monte Carlo simulations and the theoretical predictions confirms the validity of the model, providing strong evidence for the accuracy of the system under the given conditions.

The following graphs in Figures 3.3 and 3.4 present the OP for a single RIS system model over a Nakagami-m fading channel with the inclusion of the practical phase shift model. The simulations were conducted with one million samples, using the same as previous Nakagami-m parameters. Additionally, in this case, there are parameters of the reflecting elements, which were set as $\kappa_{\min} = 0$ and $\xi = 1.5$.

Figure 3.3 illustrates the OP for varying numbers of reflecting elements in the RIS, while the threshold value is fixed to 10. As expected, an increase in the number of reflecting elements leads to a reduction in the OP, demonstrating that a larger RIS array improves system performance. The inclusion of the practical phase shift model helps to account for real-world scenario, providing a more accurate depiction of system behavior compared to idealized models. The inclusion of the practical phase shift model results in slightly higher OP values, demon-

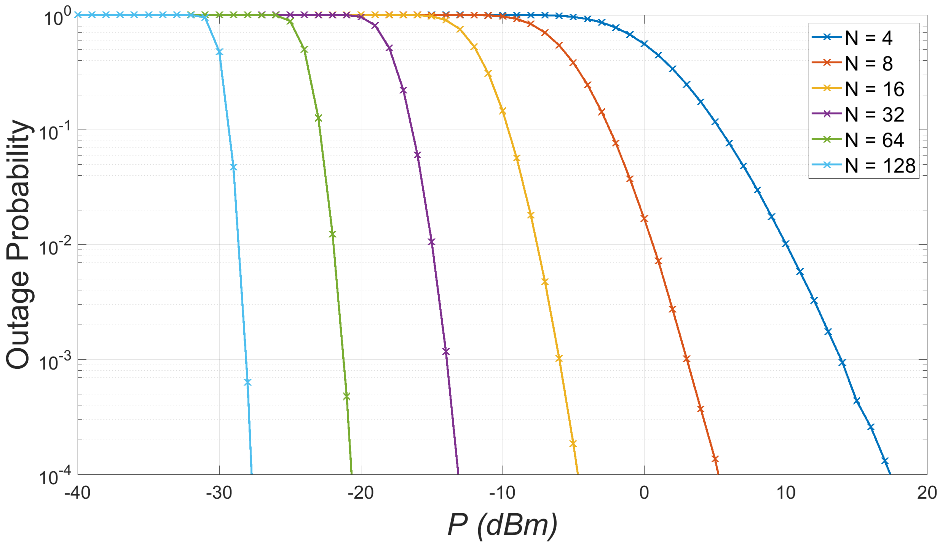

Figure 3.3: OP for a single RIS system model over a Nakagami-m fading channel with the practical phase shift model. The OP is plotted for varying numbers of reflecting elements.

strating the real-world impact of phase imperfections on system performance.

Figure 3.4 shows the OP for different threshold values, with the practical phase shift model incorporated, where number of reflecting elements are fixed to 16. As the threshold increases, the OP also increases, confirming that higher thresholds make the system more susceptible to outages by limiting the acceptable signal strength. This trend is consistent with the previous analysis, and the practical phase shift model further emphasizes the importance of considering realistic phase shifts when analyzing real-world systems, as they can impact system performance compared to idealized models.

3.2 Cascaded RIS system model over Nakagami-m fading channel

In this section, we present simulation results for the cascaded RIS system model. The following graphs depict the cascaded RIS system model, which is evaluated through Monte Carlo simulations with one million samples. Analytical derivations for these results are still in progress, and therefore, only simulation-based insights are provided here. All the channel parameters between all reflecting el-

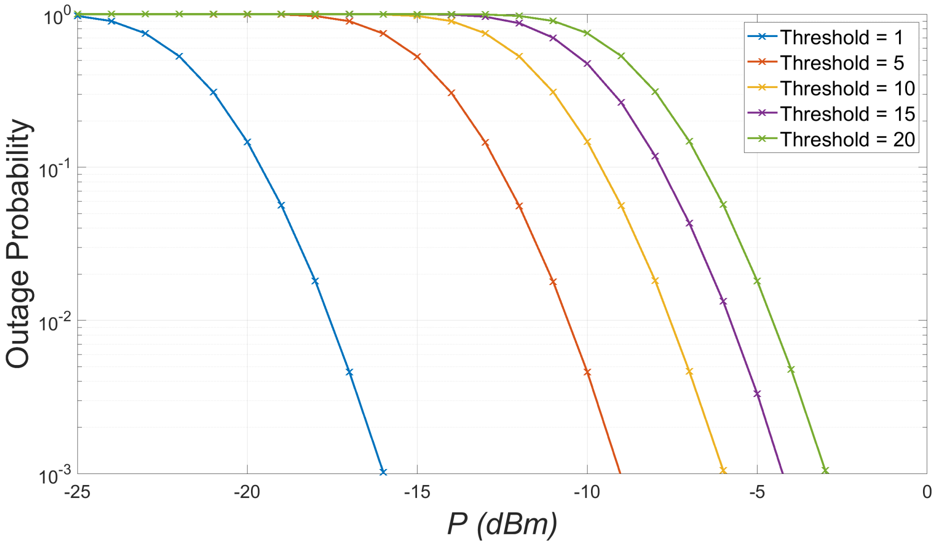

Figure 3.4: OP for a single RIS system model over a Nakagami-m fading channel with the practical phase shift model. The OP is plotted for different threshold values.

ements are modeled by Nakagami-m fading channel with unity parameters. All reflecting elements is assumed to be identical with the parameters $\kappa_{\min} = 0.2$ and $\xi = 1.6$.

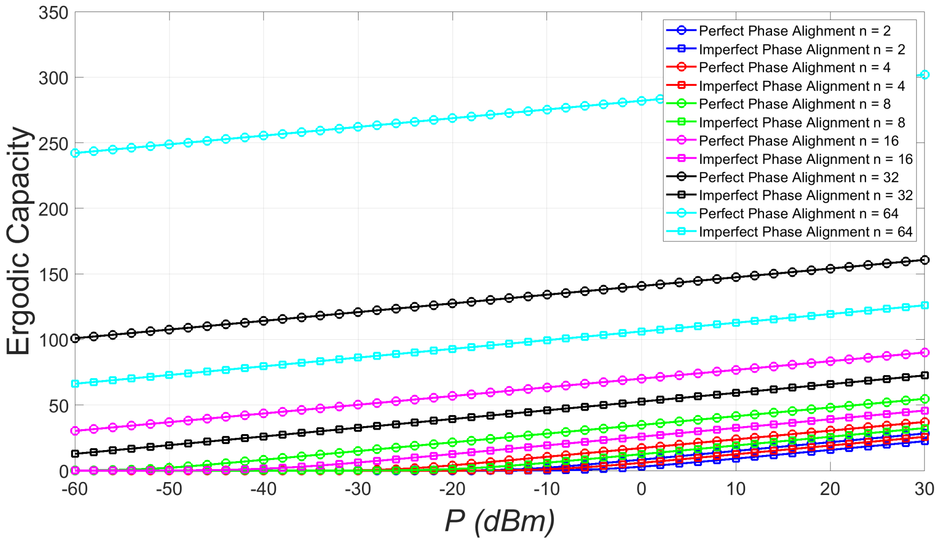

Figure 3.5: EC for the cascaded RIS system model with a fixed number of RIS layers ($n = 5$) and varying reflecting elements, considering both with and without phase errors.

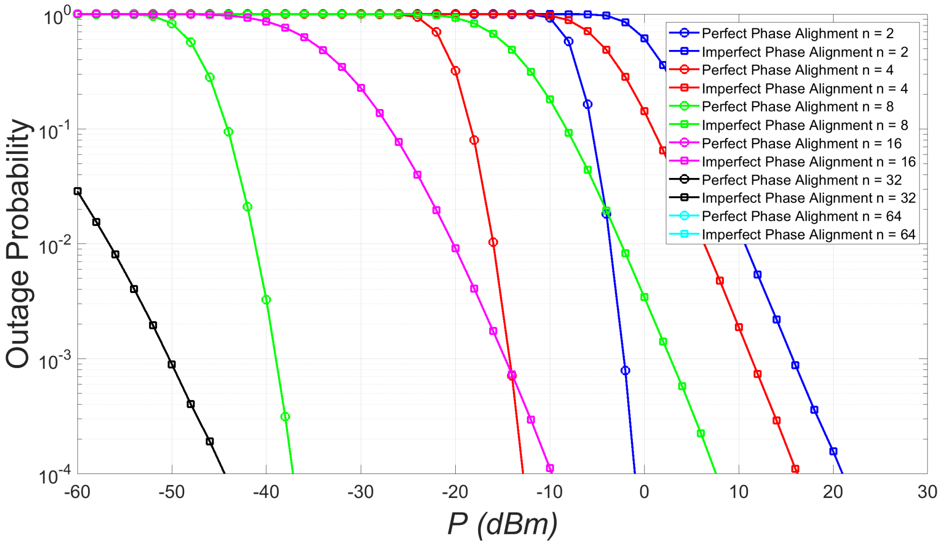

Figure 3.6: OP for the cascaded RIS system model with a fixed number of RIS layers ($n = 5$) and varying reflecting elements, considering both with and without phase errors.

Figures 3.5 and 3.6 shows the EC and OP for a cascaded RIS system with a fixed number of RIS layers ($n = 5$), while varying the number of reflecting elements. Both with and without phase errors are considered in the analysis. As observed, phase errors introduce a noticeable increase in OP and a decrease in EC, highlighting the significant impact of imperfect phase alignment on the system's performance. The results illustrate that as the number of reflecting elements increases, the EC improves, and the OP decreases. However, the performance degradation due to phase errors becomes more pronounced as the number of reflecting elements increases, emphasizing the real-world challenge of phase misalignment.

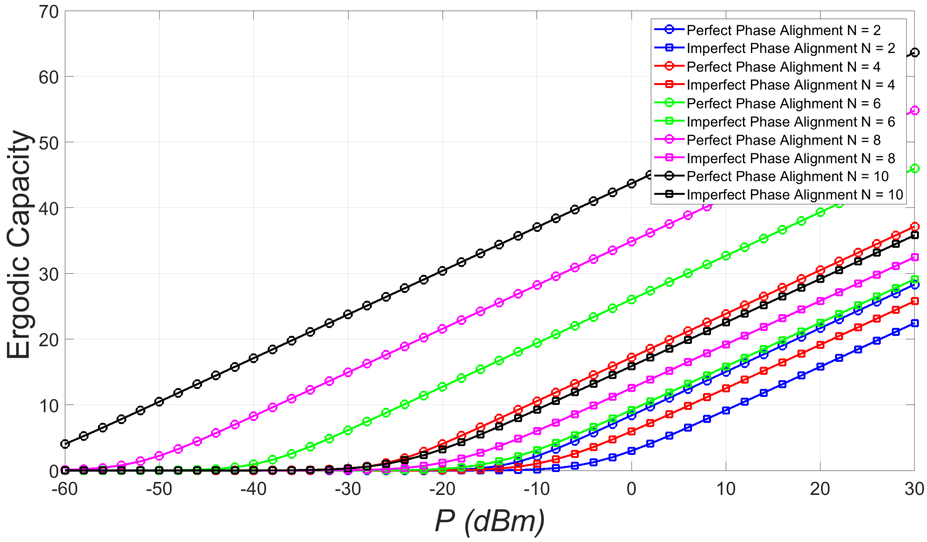

Figure 3.7: EC for the cascaded RIS system model with a fixed number of reflecting elements ($N = 10$) and varying RIS layers, considering both with and without phase errors.

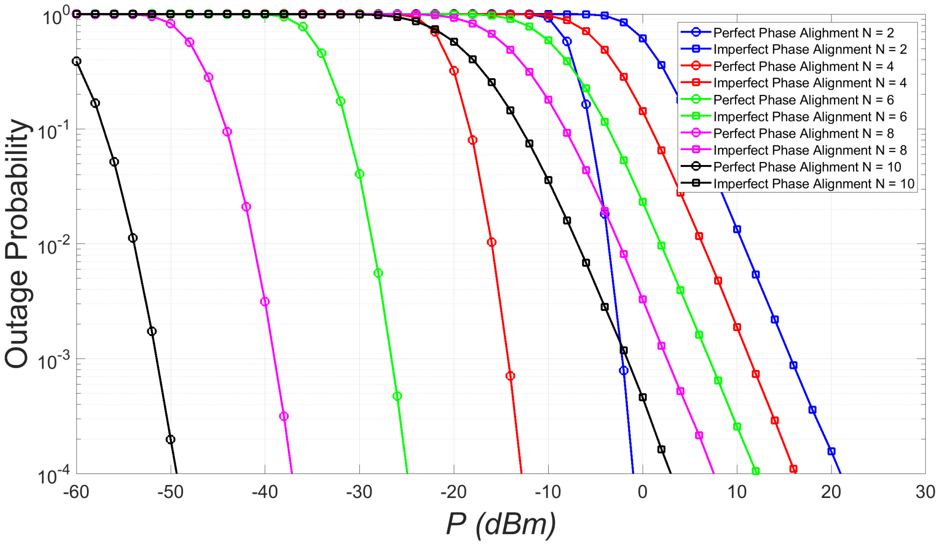

Figure 3.8: OP for the cascaded RIS system model with a fixed number of reflecting elements ($N = 10$) and varying RIS layers, considering both with and without phase errors.

Figures 3.7 and 3.8 presents the EC and OP for the same cascaded RIS system, but with a fixed number of reflecting elements ($N = 10$), while varying the number of RIS layers. Again, phase errors are considered alongside the ideal case. Similar to the previous graph, the impact of phase errors is clearly visible. As the number of RIS layers increases, both EC and OP improve, but the performance gap between the phase error and no phase error cases widens, showing that the cascading effect helps in reducing OP and increasing EC, although the phase errors still have a considerable effect on the overall system performance.

In all graphs, the key takeaway is that phase errors have a significant impact on system performance, even as the number of reflecting elements or RIS layers varies. These findings underscore the importance of considering practical imperfections in the design and analysis of RIS-based communication systems.

Chapter 4

Concluding Remarks

4.1 Summary

This thesis provides a comprehensive study of the performance analysis of cascaded RIS-based communication systems. The research focuses on evaluating key performance metrics such as OP and EC under different channel conditions, incorporating both ideal and practical phase shift models. Through analytical derivations and simulation-based evaluations, this work demonstrates the substantial potential of cascaded RIS systems. Key findings include the significant role that phase errors play in affecting system performance. While increasing the number of reflecting elements and RIS layers generally improves performance, the impact of phase shifts becomes increasingly pronounced. This insight underscores the importance of accounting for practical imperfections in RIS design, particularly when considering real-world applications where phase misalignment is unavoidable. The simulations conducted, particularly for the cascaded RIS system model, further support the theoretical predictions, although the analytical derivations for some parts of the study are still in progress. Moreover, the study highlights the importance of advanced statistical tools and analytical techniques in deriving expressions for key performance indicators, such as the multivariate Fox H-function, which was successfully used to model the Nakagami-m fading channels and phase shift distributions. The results are in perfect alignment with the analytical predictions, validating the effectiveness of the theoretical models. In conclusion, this work significantly contributes to the ongoing development of RIS technologies, providing insights into their application in advanced wireless communication systems. The findings offer valuable directions for future research, including the refinement of phase shift models and the exploration of more sophisticated fading models to further optimize the performance of RIS systems in next-generation communication networks. These advancements will be crucial for addressing the growing demands of high-capacity, low-latency communication systems envisioned for B5G and 6G networks.

4.2 Future work

Future work in this area includes several important directions for further enhancement of RIS-based communication systems. First, developing methods to find the sum of differently correlated random variables is crucial for improving the accuracy of performance metrics, such as EC and OP, in cascaded RIS models. Second, incorporating phase error into the derivations of SNR expression is essential to better account for practical imperfections and ensure more realistic performance predictions. Finally, optimizing the numerical approximation of the Fox H-function is a key challenge, as it is widely used in representing OP and EC expressions. Improving this approximation will enhance the efficiency and scalability of analysis in complex RIS systems, making it a critical area for future research.

REFERENCES

[1] A. A. A. Solyman and K. Yahya, “Evolution of wireless communication networks: from 1G to 6G and future perspective,” *International Journal of Electrical and Computer Engineering (IJECE)*, vol. 12, no. 4, pp. 3943–3950, 2022. [Online]. Available: http://ijece.iaescore.com.

[2] A. Kakkar and G. S. Nitesh, “Generations of mobile communication,” in *International Journal of Advanced Research in Computer Science and Software Engineering*, vol. 6, no. 3, 2016. [Online]. Available: https://www.researchgate.net/publication/326462813.

[3] E. Zontou, “Unveiling the evolution of mobile networks: From 1G to 7G,” *arXiv*, 2023. [Online]. Available: https://arxiv.org/abs/2310.19195.

[4] S. Akhtar, “2G-4G networks: Evolution of technologies, standards, and deployment,” *International Journal of Advanced Research in Computer Science and Software Engineering*, 2005. [Online]. Available: https://www.researchgate.net/publication/237717672.

[5] Ericsson, “The evolution of EDGE,” Ericsson AB, Tech. Rep., 2007. [Online]. Available: https://www.ericsson.com/en.

[6] B. I. Bakare and W. Abidde, “A technical review of long term evolution (LTE) operations,” *ResearchGate*, 2022. [Online]. Available: https://www.researchgate.net/publication/360086408.

[7] A. R. Nimodiya and P. N. Gulhane, “A review paper on 5G wireless technology,” *International Advanced Research Journal in Science, Engineering and Technology (IARJSET)*, vol. 9, no. 2, pp. 93–94, 2022. [Online]. Available: https://iarjset.com.

[8] D. B. da Costa and H.-C. Yang, “Grand challenges in wireless communications,” *Frontiers in Communications and Networks*, vol. 1, 2020. [Online]. Available: https://www.frontiersin.org/articles/10.3389/frcmn.2020.00001/full.

[9] R. F. Olimid and G. Nencioni, “5G network slicing: A security overview,” *IEEE Access*, vol. 8, 2020. [Online]. Available: https://doi.org/10.1109/ACCESS.2020.2997702.

[10] M. Alsabah, M. A. Naser, B. M. Mahmod, S. H. Abdulhussain, M. R. Eissa, A. Al-Baidhani, N. K. Noordin, S. M. Sait, K. A. Al-Utaibi,

and F. Hashim, “6G wireless communications networks: A comprehensive survey,” *IEEE Access*, vol. 9, pp. 148 191–148 206, 2021. [Online]. Available: https://doi.org/10.1109/ACCESS.2021.3124812.

[11] H. R. Sadjadpour, “Orthogonal frequency division multiplexing (OFDM),” *Handbook of RF and Wireless Technologies*, 2004. [Online]. Available: https://www.researchgate.net/publication/288239233.

[12] B. Rana, S.-S. Cho, and I.-P. Hong, “Review paper on hardware of reconfigurable intelligent surfaces,” *IEEE Access*, vol. 11, pp. 29 614–29 633, 2023.

[13] Y. Liu, X. Liu, X. Mu, T. Hou, J. Xu, M. Di Renzo, and N. Al-Dhahir, “Reconfigurable intelligent surfaces: Principles and opportunities,” *IEEE Communications Surveys Tutorials*, vol. 23, no. 3, pp. 1546–1568, 2021.

[14] Z. Zhakipov, K. M. Rabie, X. Li, and G. Nauryzbayev, “Accurate approximation to channel distributions of cascaded RIS-aided systems with phase errors over Nakagami-m channels,” *IEEE Wireless Communications Letters*, vol. 12, no. 5, pp. 922–926, May 2023.

[15] T. Bao, H. Wang, H.-C. Yang, W.-J. Wang, and M. O. Hasna, “Performance analysis of RIS-aided communication systems over the sum of cascaded rician fading with imperfect CSI,” in *2022 IEEE Wireless Communications and Networking Conference (WCNC)*, April 2022, pp. 399–404.

[16] I.-P. Hong, “Reviews based on the reconfigurable intelligent surface technical issues,” *Electronics*, vol. 12, p. 4489, 2023.

[17] M. Amri, “Recent trends in the reconfigurable intelligent surfaces (RIS): Active RIS to brain-controlled RIS,” *IEEE International Conference on Communication, Networks and Satellite (COMNETSAT)*, 2022.

[18] A. I. Griva, A. D. Boursianis, S. Koulouridis, P. Sarigiannidis, G. Karagiannidis, and S. K. Goudos, “Reconfigurable intelligent surfaces: A brief review on design specifications,” *13th International Conference on Modern Circuits and Systems Technologies (MOCAST)*, 2024.

[19] S. Abeywickrama, R. Zhang, Q. Wu, and C. Yuen, “Intelligent reflecting surface: Practical phase shift model and beamforming optimization,” *IEEE Transactions on Communications*, vol. 68, no. 9, pp. 5849–5863, September 2020.

[20] V. K. Chapala and S. M. Zafaruddin, “Statistical results of multivariate Fox-H function for exact performance analysis of RIS-assisted wireless communication,” *arXiv*, 2023.

[21] Y. Zhang, J. Zhang, M. D. Renzo, H. Xiao, and B. Ai, "Performance analysis of RIS-aided systems with practical phase shift and amplitude response," *IEEE Transactions on Vehicular Technology*, vol. 70, no. 5, pp. 4501–4511, May 2021.

[22] V. K. Chapala and S. M. Zafaruddin, "Intelligent connectivity through RIS-assisted wireless communication: Exact performance analysis with phase errors and mobility," *IEEE Trans. Intell. Veh.*, vol. 8, no. 10, pp. 4445–4459, Oct 2023.

[23] I. Trigui, W. Ajib, and W.-P. Zhu, "A comprehensive study of reconfigurable intelligent surfaces in generalized fading," *arXiv*, 2020.

[24] F. Almeida, F. D. P. Calmon, and J. C. S. S. Filho, "Channel characterization of RIS-aided systems over Nakagami-m fading channels: A more efficient exact approach," May 2024.

[25] D. Tyrovolas, S. A. Tegos, E. C. D. Panidou, P. D. Diamantoulakis, C. K. Liaskos, and G. K. Karagiannidis, "Performance analysis of cascaded reconfigurable intelligent surface networks," *arXiv*, 2022.

[26] M. Nakagami, *The m-Distribution—A General Formula of Intensity Distribution of Rapid Fading.* Elsevier, 1960.

[27] J. Xie and L. Li, "Outage probability and optimal power splitting ratio analysis for RIS-aided SWIPT system," in *2022 7th Asia Conference on Power and Electrical Engineering (ACPEE)*, 2022, pp. 2123–2128.

[28] I. M. Tanash and T. Riihonen, "Ergodic capacity analysis of RIS-aided systems with spatially correlated channels," in *ICC 2022 - IEEE International Conference on Communications*, 2022, pp. 3293–3298.

[29] I. S. Gradshteĭn, I. M. Ryzhik, and A. Jeffrey, *Table of integrals, series, and products*, 7th ed. Academic Press, 2007.

[30] S. Spătaru, "Generating functions for discrete distributions," *Informatica Economică*, vol. nr. 2 (42), pp. 132–137, 2007.

[31] Y. A. Rahama, M. H. Ismail, and M. S. Hassan, "On the sum of independent Fox's H-function variates with applications," *IEEE Transactions on Vehicular Technology*, vol. 67, no. 8, pp. 6752–6760, 2018. [Online]. Available: https://doi.org/10.1109/TVT.2018.2827180.

[32] A. M. Mathai, R. K. Saxena, and H. J. Haubold, *The H-Function.* Springer New York, 2010.

[33] M. Hazewinkel, Ed., *Encyclopaedia of Mathematics*, 1st ed., ser. Encyclopaedia of Mathematics. Springer Dordrecht, 1990, originally

published in Russian. [Online]. Available: https://doi.org/10.1007/978-94-009-5991-0.

[34] A. M. Makarov and A. S. Ermakov, "Method development for solving fredholm integral equations of the second kind based on the Mellin multiplicative convolution in the class of trigonometric-logarithmic functions," in *2021 Radiation and Scattering of Electromagnetic Waves (RSEMW)*, 2021, pp. 71–74.

[35] J. Bertrand, P. Bertrand, and J.-P. Ovarlez, *The Mellin Transform.* CRC Press LLC, 01 2000.

[36] M. Hazewinkel, Ed., *Encyclopaedia of Mathematics*, 1st ed., ser. Encyclopaedia of Mathematics. Springer Dordrecht, 1990, originally published in Russian. [Online]. Available: https://doi.org/10.1007/978-94-009-5991-0.

[37] H. J. Haubold, D. Kumar, and A. A. Kabeer, "Fox's H-functions: A gentle introduction through astrophysical thermonuclear functions," *arXiv preprint arXiv:2405.11325*, 2024.

[38] H. R. Alhennawi, M. M. H. El Ayadi, M. H. Ismail, and H.-A. M. Mourad, "Closed-form exact and asymptotic expressions for the symbol error rate and capacity of the H-function fading channel," *IEEE Transactions on Vehicular Technology*, vol. 65, no. 4, pp. 1957–1974, 2016.

[39] W. Research, "Meijer G-function," https://functions.wolfram.com/HypergeometricFunctions/MeijerG/02/, 2025, accessed: 2025-04-14.

APPENDICES

A Meiger G-function

The Meijer G-function is a complex function that generalizes various special functions such as hypergeometric functions, Bessel functions, and others. It is defined in terms of a contour integral in the complex plane and is used in many areas of applied mathematics, including probability theory, statistical mechanics, and the solution of differential equations. The general form of the Meijer G-function is expressed as the following contour integral

$$G_{p,q}^{m,n}\left(\begin{matrix} a_1,\ldots,a_p \\ b_1,\ldots,b_q \end{matrix}\middle| z\right) = \frac{1}{2\pi i}\int_L \frac{\prod_{j=1}^{m}\Gamma(b_j+s)\prod_{j=1}^{n}\Gamma(1-a_j-s)}{\prod_{j=m+1}^{q}\Gamma(1-b_j-s)\prod_{j=n+1}^{p}\Gamma(a_j+s)} z^{-s}\,\mathrm{d}s. \tag{A.1}$$

The Meijer G-function is defined by a contour integral, and the choice of the contour is critical for its behavior. The contour is typically denoted as L, it defines the path of integration in the complex plane and is chosen to ensure the convergence of the integral. $L = L_{\omega\pm\infty}$ is a contour starting at the point $\omega - i\infty$ and going to $\omega+i\infty$, where $\omega \in \mathbb{R} = (-\infty, +\infty)$ such that all the poles of $\Gamma(b_j+s)$, for $j = 1,\ldots,m$, are separated from those of $\Gamma(1-a_\beta-s)$, for $\beta = 1,\ldots,n$ [39].

B Fox H-function

The Fox H-function is a generalized special function that encompasses a wide range of functions, including hypergeometric functions, Meiger G-function, Mittag-Leffler functions, and others. The Fox H-function is highly versatile and can be used to express solutions to various integral equations and models in physical sciences. The general form of the Fox H-function is given by the following Mellin-Barnes integral

$$H_{p,q}^{m,n}\left[z\middle|\begin{matrix}a_1,\ldots,a_p\\ \\ b_1,\ldots,b_q\end{matrix}\right]=\frac{1}{2\pi i}\int_L\frac{\prod_{j=1}^{m}\Gamma(b_j+s)\prod_{j=1}^{n}\Gamma(1-a_j-s)}{\prod_{j=m+1}^{q}\Gamma(1-b_j-s)\prod_{j=n+1}^{p}\Gamma(a_j+s)}z^{-s}\,\mathrm{d}s. \tag{B.1}$$

where L defines the path of integration in the complex plane and is chosen to ensure the convergence of the integral. $L=L_{\omega\pm\infty}$ is a contour starting at the point $\omega-i\infty$ and going to $\omega+i\infty$, where $\omega\in\mathbb{R}=(-\infty,+\infty)$ such that all the poles of $\Gamma(b_j+B_js)$, for $j=1,\ldots,m$, are separated from those of $\Gamma(1-a_\beta-A_\beta s)$, for $\beta=1,\ldots,n$ [32].

C Multivariate Fox H-function

The multivariable H-function is a generalization of many special functions, including hypergeometric functions, Meiger G-function, and univariate Fox H-function. It is defined in terms of a contour integral referred as the Mellin-Barnes contour integral, which involves complex integration over multiple paths in the complex plane. These paths, denoted by L_1, L_2,$\cdots$, L_N, are carefully chosen to avoid singularities of the integrand, ensuring the integral converges.

$$H[z_1, \ldots, z_N] = H^{0,n:m_1,n_1;\ldots;m_N,n_N}_{p,q:p_1,q_1;\ldots;p_N,q_N}$$

$$\left[\begin{matrix} z_1 \\ \vdots \\ z_N \end{matrix} \left| \begin{matrix} (a_j;\alpha_j^{(1)},\ldots,\alpha_j^{(N)})_{1,p_1}:(c_j^{(1)},\gamma_j^{(1)})_{1,p}\ldots;(c_j^{(N)},\gamma_j^{(N)})_{1,p_N} \\ (b_j;\beta_j^{(1)},\ldots,\beta_j^{(N)})_{1,q}:(d_j^{(1)},\delta_j^{(1)})_{1,q_1}\ldots;(d_j^{(N)},\delta_j^{(N)})_{1,q_N} \end{matrix} \right. \right] = \tag{C.1}$$

$$= \frac{1}{(2\pi w)^N} \int_{L_1} \cdots \int_{L_N} \Psi(s_1, \ldots, s_N) \left\{ \prod_{i=1}^{N} \phi_i(s_i) z_i^{s_i} \right\} \mathrm{d}s_1 \ldots \mathrm{d}s_N,$$

where:

$$\Psi(s_1, \ldots, s_N) = \frac{\prod_{j=1}^{n} \Gamma\left(1 - a_j + \sum_{i=1}^{N} \alpha_j^{(i)} s_i\right)}{\left[\prod_{j=n+1}^{p} \Gamma\left(a_j - \sum_{i=1}^{N} \alpha_j^{(i)} s_i\right)\right] \left[\prod_{j=1}^{q} \Gamma\left(1 - b_j + \sum_{i=1}^{N} \beta_j^{(i)} s_i\right)\right]}, \tag{C.2}$$

$$\phi_i(s_i) = \frac{\left[\prod_{\lambda=1}^{m_i} \Gamma\left(d_\lambda^{(i)} - \delta_\lambda^{(i)} s_i\right)\right] \left[\prod_{j=1}^{n_i} \Gamma\left(1 - c_j^{(i)} + \gamma_j^{(i)} s_i\right)\right]}{\left[\prod_{j=n_i+1}^{p_i} \Gamma\left(c_j^{(i)} - \gamma_j^{(i)} s_i\right)\right] \left[\prod_{\lambda=m_i+1}^{q_i} \Gamma\left(1 - d_\lambda^{(i)} + \delta_\lambda^{(i)} s_i\right)\right]}. \tag{C.3}$$

For $i = 1, \ldots, N$, and $L_i = L_{w\tau_i\infty}$, where $w = (-1)^{\frac{1}{2}}$, represents the contours that start at the point $\tau_i - w\infty$ and extend to the point $\tau_i + w\infty$, with $\tau_i \in \mathbb{R} = (-\infty, \infty)$, and $i = 1, \ldots, N$, such that all the poles of $\Gamma\left(d_j^{(i)} - \delta_j^{(i)} s_i\right)$, $j = 1, \ldots, m_i$; $i = 1, \ldots, N$ are distinct from those of $\Gamma\left(1 - c_j^{(i)} - \gamma_j^{(i)} s_i\right)$, $j = 1, \ldots, n_i$; $i = 1, \ldots, N$ and $\Gamma\left(1 - a_j + \sum_{i=1}^{N} \alpha_j^{(i)} s_i\right)$, $j = 1, \ldots, n$ [32].